R. & M. No. 3123
(19,154)
A.R.C. Technical Report

MINISTRY OF SUPPLY

AERONAUTICAL RESEARCH COUNCIL
REPORTS AND MEMORANDA

An Approximate Method of Calculating the Laminar Boundary Layer in Two-Dimensional Incompressible Flow

By

M. R. HEAD, D.S.O., D.F.C., M.A., Ph.D.,
Department of Engineering, University of Cambridge

Communicated by PROF. W. A. MAIR

LONDON : HER MAJESTY'S STATIONERY OFFICE
1959
PRICE £1 0*s*. 0*d*. NET

An Approximate Method of Calculating the Laminar Boundary Layer in Two-Dimensional Incompressible Flow

By

M. R. HEAD, D.S.O., D.F.C., M.A., Ph.D.,
Department of Engineering, University of Cambridge*

COMMUNICATED BY PROF. W. A. MAIR

Reports and Memoranda No. 3123

March, 1957

Summary.—In the present approximate method the use of a doubly-infinite family of boundary-layer velocity profiles enables the momentum and energy integral equations of the boundary layer to be satisfied exactly, together with the first compatibility condition at the surface. The principal characteristics of the velocity profiles used have been calculated, and are presented graphically in a series of charts which enable calculations to be carried out with a minimum of labour.

Several examples of boundary-layer flow have been worked out in detail by the use of the method, and agreement with known exact solutions is in most cases extremely satisfactory. No important restrictions on the application of the method have so far appeared; in particular it has been found possible to deal successfully with certain types of flow giving rise to similar profiles and with distributed suction starting either at the leading edge or at some point downstream.

1. *Introduction.*—The present method of calculating the laminar boundary layer was developed in 1952 in connexion with proposed flight experiments on distributed suction[1]. A method was required which would be suitable for use with suction and which would give velocity profiles with sufficient accuracy to enable reliable estimates to be made of the stability of the boundary layer.

It appeared that methods based on the use of a singly-infinite family of velocity profiles would be unlikely to give the desired accuracy, not only because of difficulties arising in the prediction of separation with suction, but also because such a range of profiles could not be expected to approximate closely those which might be obtained where either suction or pressure gradient vary rapidly along the surface; in this case, whereas the general shape of the profile at any point will be largely dictated by conditions upstream, the shape in the immediate neighbourhood of the surface must conform to local boundary conditions which may be very different. As a specific example we may consider the flat plate with uniform suction following a solid-entry length; at a sufficiently short distance downstream of the discontinuity the overall profile shape will still be substantially that of the Blasius profile upstream, but in the neighbourhood of the surface the profile must be sufficiently modified to satisfy the new boundary condition. In this particular example it is obvious that any singly-infinite family of profiles intended for general use can give only a poor representation of the profiles obtained in practice, since it will be impossible in general to fit both the overall profile shape and the slope and curvature of the profile at the surface.

* Formerly at the Royal Aircraft Establishment, Farnborough, where the work leading to this paper was done.

In this case, as well as in less extreme examples, it may be expected that the use of a doubly-infinite family of profiles will give an appreciable gain in accuracy, and the examples treated in this report show this to be the case.

In the present method, which is essentially a development of an earlier method given by Wieghardt[2] for solid boundaries, the use of a doubly-infinite family of profiles enables both the energy and momentum integral equations of the boundary layer to be satisfied exactly, along with the first compatibility condition at the surface. By the use of the energy equation, the total dependence of the profile shape on local conditions (inherent in methods of the Polhausen type)[3, 4, 5] is avoided, and the influence of conditions upstream is adequately taken into account. Moreover, by continuing to satisfy the first compatibility condition at the surface, a condition which has been dropped by Walz[6], and by Wieghardt[7] in a more recent method, the necessary rapidity of response of the boundary-layer skin friction to changing conditions of pressure gradient and suction is retained, and difficulties which would otherwise arise in the accurate prediction of separation have been avoided.

The principal modifications to the original method of Wieghardt[2] consist in the use of an improved and greatly extended range of profiles and the adaptation of the method to deal with suction. The principal boundary-layer characteristics have been plotted and are presented in the form of graphs or charts; this graphical method of presentation has been adopted mainly for convenience, but in the case of H_ε (the ratio of energy to momentum thickness), it is essential for the step-by-step solution of the equations when suction is present.

The report is divided into two parts: in Part I the method is described and results obtained by its use are compared with the corresponding exact solutions; in Part II the construction of the doubly-infinite family of velocity profiles used in the method is given in some detail, along with a practical example of distributed suction applied to the upper surface of an aerofoil.

PART I

Description of the Method and Comparison with Exact Solutions

2. Description of the Method.—The momentum and energy integral equations of the incompressible laminar boundary layer in two dimensions may be written respectively

$$\frac{d\theta}{dx} = \frac{\nu}{U^2}\left(\frac{\partial u}{\partial y}\right)_0 - (H+2)\frac{\theta}{U}\frac{dU}{dx} - \frac{v_s}{U}$$

and

$$\frac{d}{dx}(U^3\varepsilon) = 2\nu\int_0^\delta \left(\frac{\partial u}{\partial y}\right)^2 dy - v_s U^2$$

where v_s is the suction velocity,

ε, the energy thickness, $= \int_0^\delta \frac{u}{U}\left\{1 - \left(\frac{u}{U}\right)^2\right\} dy$,

and the other symbols have their usual meanings*.

---

* A complete list of symbols is given at the end of Part II.

In the present method the momentum equation is used with only slight rearrangement, but, following Wieghardt[2], the energy equation is substantially modified by substitution from the momentum equation so that the rate of change of the form-parameter $H_\varepsilon (= \varepsilon/\theta)$ is given explicitly. With the introduction of a convenient dimensionless notation the momentum and energy equations then become finally

$$t^{*\prime} = \frac{2}{\bar{U}}\{l - \Lambda(H + 2) - \lambda\}, \quad \ldots \quad (1)$$

and

$$H_\varepsilon' = \frac{1}{\bar{U}t^*}[2D^* - H_\varepsilon\{l - \Lambda(H - 1) - \lambda\} - \lambda], \quad \ldots \quad (2)$$

where

$$t^* = \left(\frac{\theta}{c}\right)^2 \frac{U_0 c}{\nu},$$ c being some representative length and U_0 the free-stream velocity,

$$\bar{U} = \frac{U}{U_0}$$

$$l = \frac{\theta}{U}\left(\frac{\partial u}{\partial y}\right)_0$$

$$\Lambda = \frac{\theta^2}{\nu}\frac{dU}{dx} = t^*\bar{U}'$$

$$\lambda = \frac{\theta v_s}{\nu} = t^{*1/2} v_s^* \qquad \left(v_s^* = \frac{v_s}{U_0}\sqrt{\left(\frac{U_0 c}{\nu}\right)}\right)$$

$$H_\varepsilon = \frac{\varepsilon}{\theta}$$

$$D^* = \int_0^{\delta/\theta} \left(\frac{\theta}{U}\right)^2 \left(\frac{\partial u}{\partial y}\right)^2 d\left(\frac{y}{\theta}\right)$$

and the primes denote differentiation with respect to $\bar{x}\ (= x/c)$.

The derivation of equations (1) and (2) is given in detail in the Appendix, where it is also shown that in the presence of suction the boundary-layer equation reduces at the surface to

$$m = -(\Lambda + l\lambda), \quad \ldots \quad (3)$$

where

$$m = \frac{\theta^2}{U}\left(\frac{\partial^2 u}{\partial y^2}\right)_0$$

This represents the first compatibility condition at the surface.

Equations (1), (2) and (3) form the basis of the present method.

It will be seen that λ and Λ are parameters which depend only on θ and on known values of the local suction velocity and the velocity gradient outside the boundary layer; on the other hand D^*, H, H_ε, l and m are characteristics of the distribution of velocity within the boundary layer. For any assumed family of profiles D^*, H, H_ε, l and m may be calculated, but if the family is only singly-infinite then a unique relationship will exist between l and m, the slope and

curvature respectively of the profile at the surface, so that it is not, in general, possible to satisfy equations (1), (2) and (3); indeed it may not always be possible even to satisfy equations (1) and (3). A doubly-infinite family of profiles is therefore required, and if l and m are taken as independent variables D^*, H and H_ε may be conveniently plotted as functions of these quantities.

The construction of a doubly-infinite family of velocity profiles which covers an extremely wide range is described in detail in Part II. The characteristic quantities D^*, H and H_ε of this family have been plotted in Figs. 1 to 3 as functions of l and m. To calculate the development of the boundary layer, these three charts are used in conjunction with equations (1), (2) and (3) in the following way:

We shall first assume that starting values of t^*, l and m are given; then, by using the charts for D^*, H and H_ε, $t^{*\prime}$ and $H_\varepsilon{}'$ can readily be calculated from (1) and (2), and hence an approximation obtained to values of t^* and H_ε at a second station. From the new value of t^* and the known distributions of suction velocity and of velocity outside the boundary layer, new values of λ and Λ can be obtained; these will then correspond, according to equation (3), with a straight line which may be drawn on the chart for H_ε. The point of intersection of this straight line with the appropriate value of H_ε will give the new values of l and m. The foregoing may be expressed alternatively as follows:

The momentum and energy equations are used to find the increments in momentum thickness and H_ε respectively. From the new value of the momentum thickness, new values of λ and Λ are calculated. When these values are substituted in the boundary-layer equation at the surface, a linear relationship between l and m is obtained. The particular values of l and m which satisfy this relation and at the same time give the appropriate value of H_ε can be found by drawing the straight line representing equation (3) on the chart of H_ε. The new values of l and m so determined allow the calculation to proceed through a further step.

Once l and m are known, the corresponding velocity profile is simply obtained from the charts shown in Figs. 4 to 13.*

2.1. *Initial Values.*—Where the boundary layer starts from the leading edge in the absence of a stagnation point, as in the case of a flat plate with sharp leading edge, the momentum thickness will initially be zero and the appropriate initial values of l and m will be the Blasius values ($l = 0{\cdot}221$, $m = 0$), so long as the pressure gradient and suction velocity at the leading edge are finite. This conclusion is reached by considering that when the boundary layer is vanishingly thin the effect of pressure gradient and suction will be negligible as compared with the effects of viscosity; the exact calculations referred to in Sections 3.2, 3.3 and 3.5 (i) below support this view.

When the boundary layer starts from a stagnation point in the absence of distributed suction, l and m will take certain fixed values ($l = 0{\cdot}360$, $m = -0{\cdot}085$). The corresponding value of t^* is then simply found from the known velocity distribution and equation (3), which in this case reduces to $m = -\Lambda = -t^*\bar{U}'$.

When the boundary layer starts from a stagnation point where distributed suction is applied, use may be made of the exact calculations of Schlichting and Bussmann[10]. In Fig. 14, l and m are plotted as functions of C_0, the curves being derived from the results of these exact calculations. In the notation of the present method $C_0 = v_s^*/\sqrt{\bar{U}'}$, so that the appropriate initial values of l and m can be obtained from the given values of suction velocity and pressure gradient at the stagnation point. It can further be simply shown that $C_0 = \lambda/\Lambda^{1/2}$, so that for this case equation (3) can be written $m = -lC_0\Lambda^{1/2} - \Lambda$.

From the known values of m, l, and C_0, Λ and hence λ can be calculated.

Alternatively, if near the stagnation point arbitrary initial values of l, m, and t^* are assumed, then it may be expected (*see* Section 3.1) that these values will rapidly approach the correct ones as the calculation proceeds through a number of short steps.

* For reproduction in this report the charts were reduced in size. All, including Figs. 1, 2 and 3 which are full size, were originally drawn on graph-paper of 1 mm. squares.

The values of l and m given above have been obtained from exact solutions of the boundary-layer equations. Slightly different values would in fact correspond to the flat-plate profile and to stagnation-point profiles as determined by the present method. Differences between the exact and approximate values where these have been determined are, however, less than 2 per cent, so that the calculations should be virtually unaffected by the choice of either exact or approximate starting values of l and m.

2.2. *Simplifications Resulting from the Absence of Suction.*—It will be noted that in the absence of distributed suction equation (3) reduces to $m = -\Lambda$, so that once increments in t^* and H_ϵ have been calculated the appropriate values of l and m follow more readily than in the general case.

A more important simplification is indeed possible, since equations (1) and (2) may be written for this case

$$t^{*\prime} = \frac{2}{\bar{U}} F_1(l, \Lambda) \quad .. \quad .. \quad .. \quad .. \quad .. \quad .. \quad (4)$$

$$H_\epsilon' = \frac{1}{\bar{U}t^*} F_2(l, \Lambda) \, . \quad .. \quad .. \quad .. \quad .. \quad .. \quad .. \quad (5)$$

For any given family of velocity profiles F_1 and F_2 may be calculated once for all and presented in the form of tables or graphs. Wieghardt[2] has in fact provided such tables derived from a doubly-infinite family of profiles discussed in Part II.

It will be seen that when distributed suction is present, functions corresponding to F_1 and F_2 will contain three variables, so that they cannot be readily tabulated or graphed. For this reason it has been necessary in developing the general method to take the indirect course of plotting the relevant boundary-layer characteristics as functions of l and m, these being determined jointly as we have seen, by H_ϵ, λ and Λ.

2.3. *Difficulties Arising in the Use of the Method.*—In general it is not known initially how to extrapolate H_ϵ' and $t^{*\prime}$ to the middle of the first step; one trial is, however, normally sufficient to establish the appropriate extrapolated values. A more serious difficulty arises when the boundary layer is thin, *i.e.*, for small values of t^*. In this case it may be found that successive values of H_ϵ' tend to oscillate wildly and considerable difficulty may be experienced in maintaining a smooth curve of H_ϵ' plotted against $\bar{x}$. In this case it will be necessary to reduce the increments in $\bar{x}$ and to use considerable care in reading values from the charts.* In fact, it has so far been found that such divergencies as occur with careful working do not seriously affect the accuracy of the result, and it is only rarely that extrapolated values of H_ϵ' have been revised to obtain a smoother curve.

2.4. *Example.*—In Section 10 the case is considered of suction applied in an adverse pressure gradient. Figs. 15 and 16 show the results of the calculations for a particular distribution of suction velocity. It will be seen from Fig. 15 that there is a considerable scatter in the values of H_ϵ', though H_ϵ and t^* lie on relatively smooth curves. The example is referred to here to show the order of accuracy with which the examples that follow have in general been treated. In carrying out the calculations it has been found that if both suction and pressure gradient are present, then each step requires 7 to 15 minutes to complete. If, on the other hand, either suction or pressure gradient alone is present, then this time is approximately halved.

3. *Comparison of Results Obtained by the Present Method with Known Exact Solutions.*—3.1. *Schubauer's Ellipse.*—The experimental pressure distribution and point of separation observed on an ellipse[13] have been used as a test of approximate methods of calculating the laminar boundary layer. Both Howarth[8] and Hartree[14], the latter using a differential analyser, have obtained solutions which do not give separation near that observed experimentally.

* *See* footnote on previous page.

However, by very slightly modifying the observed pressure distribution, solutions are obtained which give good agreement with experiment. The sensitiveness of the position of separation to the exact value of the pressure gradient in this region, which may not have been determined experimentally with a sufficiently high degree of precision, limits the usefulness of this method of testing the accuracy of the approximate solutions. However, the solution obtained by Hartree[14], which should be very nearly exact for the pressure distribution which he assumed, may be used for comparison. The present method has been applied using the modified pressure distribution given by Hartree.

At a distance around the surface from the stagnation point equal to $0{\cdot}001$ (in terms of the semi-minor axis of the ellipse) the following starting values, known to be very different from those appropriate to stagnation, were assumed:

$$\left.\begin{aligned} l &= 0{\cdot}221 \\ m &= 0 \end{aligned}\right\} \text{ Blasius values}$$

$$\frac{\theta^2}{\nu} = {\cdot}001 \, .$$

After 15 steps, starting with intervals of $x = 0{\cdot}00002$, the following values, which changed only slowly with x, were obtained near $x = 0{\cdot}0017$:

$$l = 0{\cdot}365$$

$$m = -\,0{\cdot}085$$

$$\frac{\theta^2}{\nu} = 0{\cdot}0097.$$

The profile corresponding to these values is compared in Fig. 17 with the stagnation-point profile given by Howarth[8]. It will be seen that the agreement is excellent. It therefore appears that, at least in the region of the stagnation point, the method is self-correcting to a remarkable degree.

The remainder of the solution is compared in Figs. 18 to 20 with that obtained by Hartree. Velocity profiles at separation are not compared, since profiles are not given by Hartree for the pressure distribution modified beyond $x = 1{\cdot}8$. It will be seen that the general agreement is extremely satisfactory; however, the present method gives a slight delay in separation and values of skin friction for $x < 0{\cdot}2$ which are in general greater than those given by Hartree.

3.2. *Howarth Flow* ($U = b_0 - b_1 x$).—Howarth[8] has given an exact solution of the laminar boundary-layer equations for the case where the stream velocity decreases linearly with the distance along the surface. Here, since there was no stagnation point, the Blasius values of l and m were used to start the calculation by the present method. After eleven steps a separation profile was obtained. In Figs. 21 to 24 the results of the calculations are compared with those of Howarth, the notation used being that of the original author. The general agreement will again be seen to be extremely satisfactory.

3.3. *Circular Cylinder.*—In 1911 Hiemenz[15] gave the results of an experiment in which the point of laminar separation on a circular cylinder was observed and compared with the position calculated using a Blasius series. The observed velocity distribution outside the boundary layer was approximated for the calculation by a fifth-degree polynomial in x, the distance around the surface from the stagnation point. Görtler discusses the calculations of Hiemenz in Refs. 16 and 17, and concludes that the results may be regarded as a good approximation up to $x = 4{\cdot}5$, at which point Görtler commences his calculations by his own method of differences using the same approximation for the distribution of external velocity as had been used by Hiemenz. This distribution has also been used for calculations by the present method, the results of which are compared with those of Görtler in Figs. 26 and 27. Two sets of calculations were in fact performed

by the present method, one starting at the stagnation point and the other at $x = 4{\cdot}5$, using one of the initial profiles given by Görtler. Both sets of calculations gave separation at $x = 6{\cdot}825$. The following lists the positions of separation as calculated by various methods:

	Pohlhausen	6·94	From Ref. 2
	Blasius and Hiemenz	6·98	
	Wieghardt (from $x = 5{\cdot}5$)	6·77	
Difference methods	Schröder	6·87	
	Görtler (1939)	6·77	
	Görtler (1944)	6·80	
	Thwaites[18]	6·63	Calculated by present author
	Present method	6·825.	

From these results and those shown in Figs. 26 and 27 it may be concluded that the present method is comparable in accuracy with those based on the step-by-step solution of the boundary-layer equation.

3.4. *Flat Plate with Uniform Suction.*—For this case equations (1), (2) and (3) are most conveniently put in the form

$$\lambda^{2\prime} = 2(l - \lambda)\,, \qquad \ldots \qquad (6)$$

$$H_\varepsilon{}' = \frac{1}{\lambda^2}\{2D^* - H_\varepsilon(l - \lambda) - \lambda\}\,, \qquad \ldots \qquad (7)$$

where the primes denote differentiation with respect to $\xi(= (v_s/U)^2 R_x)$, and $m = -l\lambda$.

The results obtained by the present method are compared in Figs. 28 to 30 with the exact solution given by Iglisch[19]. The discrepancies between the exact and approximate values of $v_s\theta/\nu$ and $v_s\delta^*/\nu$, though probably of no great practical importance, are somewhat surprising in view of the fact that the asymptotic profile was one of the four known profiles used to build up the doubly-infinite family which forms the basis of the method. There are probably two complementary reasons for the discrepancy; one is the only moderate degree of accuracy with which the characteristics D^* and H_ε have been determined from the profiles, and the other is the sensitiveness of the solution to the exact course of the l, m path traversed. The momentum equation may, for this problem, be put in the form

$$\lambda^{2\prime} = 2\left(l + \frac{m}{l}\right).$$

The small difference between the exact and the approximate l, m paths, which arises from the inaccuracies in D^* and H_ε mentioned above, is then responsible for the relatively larger discrepancies in $v_s\theta/\nu$ and in $v_s\delta^*/\nu$. The exact and approximate l, m paths are shown in Fig. 31.

The asymptotic behaviour of the solution is particularly satisfactory, values of l and m being approached at which $\lambda^{2\prime}$ and $H_\varepsilon{}'$ simultaneously vanish. These asymptotic values of l and m are somewhat different from the exact values ($l = 0{\cdot}512$, $m = 0{\cdot}263$ instead of $0{\cdot}50$ and $0{\cdot}25$ respectively), due again to small inaccuracies in the values of D^* and H_ε.

3.5. *Flat Plate with Uniform Suction following a Solid-Entry Length.*—Exact solutions to this problem have been found by Watson[20] for different lengths of solid entry, though these solutions have not been carried far downstream. The approximate results obtained by the present method are compared with Watson's results in Figs. 32 to 34. The approximate calculations were started at the commencement of suction, up to which point the normal Blasius solution was used.

If the results are compared with those which have been, or which might be, obtained by approximate methods based on the use of the momentum equation alone it will be seen that very considerable advantages arise in this case from the joint use of the momentum and energy equations. As an extension of their methods applied to the flat plate with uniform suction, both Schlichting[21] and Preston[22] have presented approximate solutions for the flat plate with solid entry. While Preston's solution is extremely satisfactory for the flat plate with uniform suction the results obtained with a solid entry can be considered approximately correct only at a considerable distance downstream; at the commencement of suction there is a large discontinuity in δ^* and the general behaviour in this region does not compare with the exact solution. The method of Thwaites may be expected to give results very close to those obtained by Preston, since again the value of λ at any point alone determines the boundary-layer characteristics and the subsequent development of the boundary layer. Thus, to take a particular example, if, by adjusting the length of solid entry, or the rate of suction, so that λ has the same value at the commencement of suction as is asymptotically approached far downstream, then at the beginning of suction the boundary layer will immediately take the asymptotic form. This represents a very considerable discontinuity in profile shape and displacement thickness.

In the present method the values of both momentum and energy thicknesses are preserved constant at the discontinuity. Thus, for the flat plate with solid entry, the starting point of any calculation in the suction region lies on the line of constant H_e which has the Blasius value and is fixed by the value of λ at the beginning of suction. Fig. 55 shows the l, m paths traced out in the course of the calculations and Fig. 36 a comparison between the Blasius profile and the profiles at the commencement of suction. It will be seen that the discrepancies are small.

3.6. *Similar Profiles.*—In certain types of flow, boundary-layer velocity profiles are obtained which, expressed in the appropriate non-dimensional terms, are identical at all points along the surface. A particular example of this type is the Blasius solution for the flat plate, which as shown by Preston[22] and by Schlichting and Bussmann[10], applies also when distributed suction is applied in such a manner that $v_s = Kx^{-1/2}$; only the boundary condition at the surface is then altered, the Blasius equation itself remaining unchanged. More generally, for solid boundaries, the pressure distributions represented by $U = Cx^n$ give rise to similar profiles and in this case also, as pointed out by Preston[22], a distribution of suction can be found for any value of n which will give an ordinary differential equation of the same form as for zero suction. As mentioned previously, Schlichting and Bussmann [10] give results for the case where $n = 1$ (stagnation-point flow) and solutions for the general case are given by Mangler in Ref. 23, which contains a very full and detailed discussion on the subject of similar profiles. Thwaites[24] gives a large number of solutions obtained by relaxation methods and uses these as the basis of an approximate method of calculating the laminar boundary layer with suction.

In this Section the present approximate method is used to investigate the families of similar profiles obtained:

(*a*) in the absence of a pressure gradient

(*b*) in the absence of distributed suction

(*c*) with both suction and pressure gradient.

(*a*) *Similar profiles in the absence of a pressure gradient.*—For each member of a family of similar profiles l and m must take values which are independent of x. This immediately implies $H_e' = 0$. In the absence of a pressure gradient this condition becomes (*see* equation (2)):

$$0 = 2D^* - H_e(l - \lambda) - \lambda \,. \qquad (9)$$

For given values of l and m, D^* and H_e may be obtained from the appropriate charts and λ determined from equation (3) which in this case reduces to:

$$\lambda = -\frac{m}{l}. \qquad (10)$$

Thus for a series of values of l we can plot the right-hand side of (9) against m, and hence for each value of l find the corresponding value of m which satisfies the equation. The values of m so obtained are found when plotted against l to lie on a smooth curve which defines the family of similar profiles. This curve is shown in Fig. 37.

We may now use the momentum equation and equation (10) to find the distribution of suction velocity which gives rise to similar profiles and to find the rate of suction corresponding to any given profile in the singly-infinite series.

The momentum equation may be written for this case

$$\frac{d}{dx}\left(\frac{\theta^2 U}{\nu}\right) = 2(l - \lambda) ,$$

and for any given profile in the family of similar profiles, l and m, and hence l and λ, are constant, so that

$$\frac{\theta^2 U}{\nu} = 2(l - \lambda)x ,$$

or

$$\frac{\theta}{x} = \sqrt{\{2(l - \lambda)\}} R_x^{-1/2} . \quad .. \quad .. \quad .. \quad .. \quad .. \quad (11)$$

Also, by definition, $\lambda = \theta v_s/\nu$.

Hence we obtain

$$\frac{v_s}{U} = \frac{\lambda}{\sqrt{\{2(l - \lambda)\}}} R_x^{-1/2} . \quad .. \quad .. \quad .. \quad .. \quad .. \quad (12)$$

In the absence of a pressure gradient, similar profiles are therefore obtained when the suction velocity varies as $x^{-1/2}$, the boundary-layer thickness then being proportional to $x^{+1/2}$. This result is, or course, the same as that given by exact theory.

For any given profile in the family of similar profiles defined by the l, m curve obtained above we can calculate from (10) and (12) the rate of suction (defined by $v_s/U\sqrt{R_x}$) which gives rise to it. By plotting l and m as functions of $v_s/U\sqrt{R_x}$ we may then conversely find the values of l and m corresponding to a given rate of suction. Once l and m are known, the values of $\theta\sqrt{(U/\nu x)}$, H and $\delta^*\sqrt{(U/\nu x)}$ readily follow.

In Figs. 38 and 39 results obtained by the present method are compared with differential-analyser solutions given by Thwaites[9]. It will be seen that the agreement is excellent throughout.

As an alternative method of attack the distribution of suction velocity given by $v_s/U\sqrt{R_x} = 1$ was taken, and initial values of l, m and t^* chosen which were very different from those corresponding to the final profile. After approximately 20 steps the appropriate stationary values of l, m and t^* were achieved.

(*b*) *Similar profiles in the absence of suction.*—Falkner and Skan[11] show that for the flow represented by $U = Cx^n$ the boundary-layer equation is reduced to an ordinary differential equation. Hartree[12] has given numerical solutions of this equation for various values of β $(= 2n/(n + 1))$. Each value of β corresponds to a boundary-layer velocity profile which, expressed in the appropriate non-dimensional terms, is identical at all points along the surface.

The problem of similar profiles obtained without suction by a suitable distribution of external velocity will be examined by the present approximate method.

For any profile in the family of similar profiles l and m must be constant, so that $H_\varepsilon' = 0$. Thus, for this case,

$$0 = 2D^* - H_\varepsilon(l - (H - 1)\Lambda) .$$

As before, we find the l, m curve representing the family of velocity profiles by finding for a series of values of l the corresponding values of m for which this equation is satisfied. The l, m curve obtained in this way extends from $l = 0$ to $l = 0{\cdot}6$, the limit of the charts, and is shown in Fig. 40 along with other curves discussed later.

From the momentum equation and the boundary-layer equation at the surface we can once again deduce the necessary condition for similar profiles, and at the same time find the flow which gives rise to any particular profile in the series defined by the l, m curve.

The momentum equation may be written for this case

$$\frac{d}{dx}\left(\frac{\theta^2}{\nu}\right) = \frac{2}{U}\{l - \Lambda(H+2)\}\,.$$

Now, since $m(= -\Lambda)$ is constant,

$$\frac{\theta^2}{\nu} = -\frac{m}{dU/dx}\,,$$

so that

$$-\frac{d}{dx}\left(\frac{m}{dU/dx}\right) = \frac{2}{U}\{l - \Lambda(H+2)\}\,,$$

or

$$\frac{d^2U}{dx^2} + \frac{k}{U}\left(\frac{dU}{dx}\right)^2 = 0\,, \qquad \ldots\ldots\ldots\ldots\ldots\ldots\ldots \quad (13)$$

where

$$k = -\frac{2}{m}\{l - \Lambda(H+2)\}\,. \qquad \ldots\ldots\ldots\ldots \quad (14)$$

A solution to equation (13) is $U = Cx^n$, where $n = 1/(k+1)$ and C is a constant.

Thus, as is otherwise known from exact solution of the boundary-layer equations, the flow $U = Cx^n$ gives rise to similar profiles.

At any point along the l, m curve provisionally defining the family of profiles, the value of k can be simply found from (14) by the use of the appropriate charts, the value of Λ being for this case $-m$.

From the values of k the corresponding values of n and β readily follow. In Fig. 40, m, k, n, and β are plotted as functions of l. This Figure is of some interest and will be further discussed later.

Hartree presents his results in the form of velocity profiles expressed in terms of variables which we shall call Y and u/U in order to avoid confusion with the notation so far used.

From the transformations used by Hartree it follows that

$$Y = \frac{y}{x}\left(\frac{Ux}{\nu}\right)^{1/2}\{\tfrac{1}{2}(n+1)\}^{1/2}$$

To compare results obtained by the present method with those given by Hartree, values of l and m corresponding to Hartree's values of β were determined from Fig. 40 and hence from the appropriate charts velocity profiles in terms of y/θ. Values of y/θ were then transformed to values of Y in the following way:

Since, for this case,
$$m = -\Lambda = -\frac{\theta^2}{\nu}\frac{dU}{dx}$$

$$\theta = \left(-\frac{m\nu}{dU/dx}\right)^{1/2}$$

$$= \left(-\frac{m\nu}{nCx^{n-1}}\right)^{1/2}$$

$$= \left(-\frac{m}{n}\frac{\nu x}{U}\right)^{1/2}$$

or

$$\frac{\theta}{x}\left(\frac{Ux}{\nu}\right)^{1/2} = -\left(\frac{m}{n}\right)^{1/2}. \qquad \ldots\ldots\ldots\ldots\ldots\ldots \quad (15)$$

Thus

$$Y = \frac{y}{\theta}\frac{\theta}{x}\left(\frac{Ux}{\nu}\right)^{1/2}\{\tfrac{1}{2}(n+1)\}^{1/2}$$

$$= \frac{y}{\theta}\left[-\frac{m}{2n}(n+1)\right]^{1/2}.$$

For the given values of β, m and n were determined and hence velocity profiles found which are compared with those given by Hartree in Fig. 41.

In Ref. 25 Mangler tabulates the relevant characteristics H, l and m of the Hartree profiles as functions of β. He also gives the values of momentum and displacement thickness expressed in the same units of length as Y. Thus we define

$$\Theta = \frac{\theta}{x}\left(\frac{Ux}{\nu}\right)^{1/2}\{\tfrac{1}{2}(n+1)\}^{1/2}$$

and

$$\Delta^* = \frac{\delta^*}{x}\left(\frac{Ux}{\nu}\right)^{1/2}\{\tfrac{1}{2}(n+1)\}^{1/2}$$

From (15) we see that

$$\Theta = \left[-\frac{m}{2n}(n+1)\right]^{1/2},$$

so that for any given value of β, knowing n and m, we can simply find Θ; the corresponding value of Δ^* then follows from the value of H, which can be determined from the known values of l and m. Results obtained by the present method are compared with those given by Mangler in Fig. 42.

Reverting now to Fig. 40, we notice that β is a smooth function of l but that there is an infinite discontinuity in k at $l = 0{\cdot}224$ and in n at $l = 0{\cdot}398$. The discontinuity in k with change of sign corresponds simply to n passing through zero from small negative to small positive values. This change in sign of n is accompanied by a corresponding change in the sign of m, as might be expected since

$$m = -\Delta = -\frac{\theta^2}{\nu}\frac{dU}{dx} = -\frac{\theta^2}{\nu}(nCx^{n-1}).$$

Thus, no anomaly results from the discontinuity in k. At $l = 0{\cdot}398$, however, n passes from a large positive to a large negative value without any corresponding change in the sign of m, and the negative values of n obtained for $l > 0{\cdot}398$ are clearly incompatible with the negative values of m for which k (and hence n and β) were calculated in this region. This anomalous result leads to the conclusion that for values of l greater than $0{\cdot}398$ ($\beta > 2$), real solutions for the flow $U = Cx^n$ do not exist*. It will be noted that the profile represented by $l = 0{\cdot}398$, $m = -0{\cdot}109$ ($\beta = 2$) is now the limiting profile, which is asymptotically approached as n is increased without limit. The profile at $m = -0{\cdot}085$ ($n = 1$, $\beta = 1$) is the stagnation-point profile in the absence of suction (*cf.* Section 3.1) and the profile at $l = 0{\cdot}224$, $m = 0$ ($n = 0$, $\beta = 0$) corresponds to the Blasius solution for the flat plate. The values of l and m given are, of course, approximate and represent the results obtained by the application of the present method.

(*c*) *Similar profiles with suction and pressure gradient.*—Using the present method it is easy to find the 'similar' profile which corresponds to given values of λ and Δ. The values of λ and Δ will define a line on the l, m chart according to equation (3). If, for various points along this line, the expression for $H'\bar{U}t^*$ is calculated, the various points of l and m for which $H' = 0$ can be simply found by plotting. These values will define the 'similar' profile corresponding to the given values of λ and Δ.

---

* Since the above was written it has been pointed out to the author that the profiles beyond $l = 0{\cdot}398$ represent solutions for the flow $U = C(x - x_0)^n$, where $x - x_0 < 0$, as given by Mangler (Zeitschrift für angewandte Mathematik und Mechanik, Vol. 23, pp. 241 to 245. 1943).

By following the above procedure for a series of values of λ and Λ given by Thwaites, it was possible to find the corresponding family of similar profiles. In Figs. 43 and 44 these are compared with the profiles given by Thwaites[24]. It will be seen that the agreement is excellent.

3.7. *Comments.*—In all the foregoing examples the general behaviour of the boundary layer as calculated by the present approximate method is in excellent agreement with that calculated exactly; quantitatively also the results are of acceptable accuracy. Such discrepancies as exist are almost certainly due in the main to the limited accuracy with which the boundary-layer characteristics have been determined, and by slight modification the charts could be made to give results which agree even more closely with the exact solutions. Once a start had been made in using the method, however, it was considered advisable to keep the charts unaltered, and to present these with the examples for which they had been used.

PART II

Construction of Charts and Calculations Applied to an Aerofoil with Suction

4. *Construction of a Doubly-infinite Family of Velocity Profiles.*—4.1. *Wieghardt's Profiles.*—In Wieghardt's method[2], the following polynomial is used to represent the distribution of velocity in the boundary layer:

$$\frac{u}{U} = 1 - (1 - \eta)^8(1 + A_1\eta + A_2\eta^2 + A_3\eta^3) .$$

Here $\eta = y/\delta$.

It will be seen that the first seven derivatives of u with respect to η vanish at the edge of the boundary layer, where $u/U = 1$.

A_1, A_2, and A_3 are determined to satisfy three boundary conditions at the surface, and the expression for u/U reduces to

$$\frac{u}{U} = f_1 + af_2 + bf_3 ,$$

where f_2 and f_3 are functions of η for which $f_2''(0) = f_3'(0) = 0$ and a and b are form parameters which are simply related to the slope and curvature respectively of the profile at the surface.

The functions of f_1, f_2, and f_3 which follow from the polynomial chosen by Wieghardt are shown in the accompanying sketch.

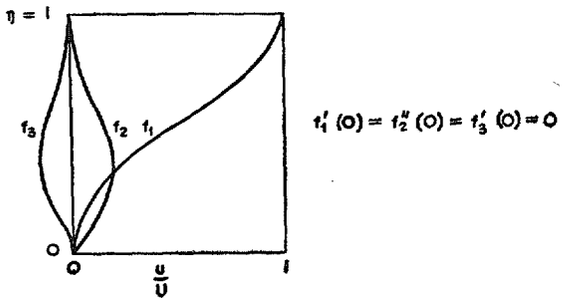

It will be seen that f_1 may be regarded as a basic profile to which varying amounts of the functions f_2 and f_3 may be added independently to modify the slope and curvature respectively of the profile at the surface. The range of profiles which may be built up in this way is considerable, but unfortunately does not extend to the more stable convex profiles which may be obtained

with suction or in a favourable pressure gradient. Moreover, the fit with known profiles for given values of l and m is by no means perfect. This latter shortcoming may not be considered serious, nor is the limited range of profiles of great importance in solid-boundary problems, since one-parameter methods can be conveniently used in this case for calculations in regions of falling pressure. Such methods cannot, however, be used with the same confidence to calculate the convex profiles which may be obtained with distributed suction even in regions of rising pressure.

4.2. *Present Method of Constructing Profiles.*—For the reasons given at the end of the previous Section it appeared that if Wieghardt's method was to be extended to enable calculations to be carried out on the laminar boundary layer with suction, a considerably extended range of profiles would be required. To obtain such an extended range of profiles the principle of adopting a basic profile and of modifying this by adding varying amounts of functions f_2 and f_3 was retained, but the representation of profiles in analytic terms was abandoned and f_1, f_2 and f_3 defined numerically. In addition, f_1 was taken as the Blasius profile and f_2 and f_3 determined in such a way that approximate profiles were obtained which fitted exactly two known profiles other than the Blasius. The method by which f_2 and f_3 were found to satisfy these known profiles is outlined in the following section.

4.3. *Determination of Functions f_2 and f_3.*—We assume that a doubly infinite family of velocity profiles is represented by

$$\frac{u}{U} = f(\eta) = f_1(\eta) + cf_2(\eta) + df_3(\eta) ,$$

where $\eta = y/\delta$, $f_1(\eta)$ is the Blasius profile ($f_1''(0) = 0$), $f_2''(0) = f_3'(0) = 0$, and c and d are constants which determine the shape of the profile. The functions f_2 and f_3 are as yet unknown but may be expected to appear somewhat as shown in the accompanying sketch.

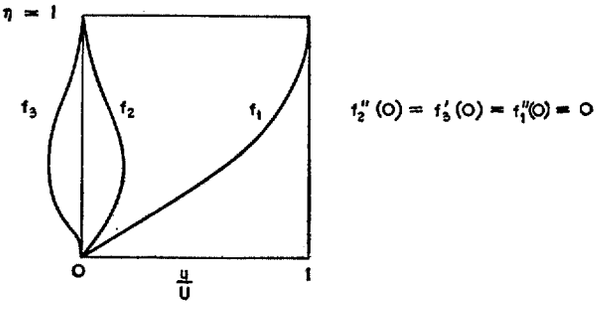

Our object is to determine f_2 and f_3 in such a way that two approximate profiles given by

$$\frac{u}{U} = f_1 + c_1 f_2 + d_1 f_3 \quad .. \quad .. \quad .. \quad .. \quad .. \quad .. \quad (1)$$

and

$$\frac{u}{U} = f_1 + c_2 f_2 + d_2 f_3 \quad .. \quad .. \quad .. \quad .. \quad .. \quad .. \quad (2)$$

can be fitted exactly (when c and d are given the appropriate values) to two given profiles represented by

$$\frac{u}{U} = F(\eta) \quad .. \quad .. \quad .. \quad .. \quad .. \quad .. \quad .. \quad .. \quad (3)$$

and

$$\frac{u}{U} = G(\eta) \text{ respectively.} \quad .. \quad .. \quad .. \quad .. \quad .. \quad .. \quad (4)$$

We start by assigning arbitrary values to $f_2'(0)$ and $f_3''(0)$. Then from the following equations c_1, d_1, c_2 and d_2 are so determined that the approximate profiles fit the given profiles at the origin.

$$F'(0) = f_1'(0) + c_1 f_2'(0)$$
$$F''(0) = d_1 f_3''(0)$$
$$G'(\eta) = f_1'(0) + c_2 f_2'(\eta)$$
$$G''(0) = d_2 f_3''(0) .$$

These equations follow readily from (1), (2), (3), and (4), and the fact that

$$f_1''(0) = f_2''(0) = f_3'(0) = 0 .$$

For any given value of η (say η_1), we can find values of f_2 and f_3 which will make the approximate profiles fit the given profiles at this value of η. It will be seen that the equations to be satisfied are

$$F(\eta_1) = f_1(\eta_1) + c_1 f_2(\eta_1) + d_1 f_3(\eta_1)$$
$$G(\eta_1) = f_1(\eta_1) + c_2 f_2(\eta_1) + d_2 f_3(\eta_1) .$$

All quantities in these equations are known, other than $f_2(\eta_1)$ and $f_3(\eta_2)$, so that numerical values of these latter quantities readily follow.

By repeating the procedure of the last paragraph for a sufficient number of values of η we can determine the complete profiles of f_2 and f_3.

Functions f_2 and f_3 have now been determined in such a way that by giving appropriate values to c and d, approximate profiles are obtained which fit exactly the given profiles. It may be expected further that by the use of these functions a close approximation may be obtained to any profile which is generally similar to the given profiles. This is in fact found to be the case.

It will be remembered that in the first instance $f_2'(0)$ and $f_3''(0)$ were given arbitrary values from which c and d followed; equally it is possible to assign arbitrary values to c and d which will determine corresponding values of $f_2'(0)$ and $f_3''(0)$.

It is found in practice that f_2 and f_3, as determined from two profiles at or near separation, are different from those determined from two profiles with high skin friction. This difference is exemplified in Figs. 45 and 46, where it will be seen that for the same values of $f_2'(0)$ and $f_3''(0)$ values of f_2 and f_3 are smaller in general in the second case. This implies that given changes in $1/U\ (\partial u/\partial \eta)_0$ or in $1/U\ (\partial^2 u/\partial \eta^2)_0$ result in greater overall changes in profile when the skin friction is small.

4.4. *Detailed Procedure Adopted.*—The functions f_2 and f_3 were found from two separation profiles given by Thwaites[24], and from the asymptotic suction profile and a hypothetical profile having the same value of $1/U\ (\partial u/\partial \eta)_0$ but with $1/U\ (\partial^2 u/\partial \eta^2)_0 = 0$. We shall use the subscript $_1$ to refer to f_2 and f_3 as determined from the separation profiles and the subscript $_2$ for those functions determined from the profiles with high skin friction.

c and d were arbitrarily given the value unity for the asymptotic suction profile; the values of c and d corresponding to the separation profiles were then determined to make

$$[f_2'(0)]_1 = [f_2'(0)]_2$$

and

$$[f_3''(0)]_1 = [f_3''(0)]_2$$

Thus for the two profiles with high skin friction $c = 1$, and for the two separation profiles it was found that $c = -0{\cdot}493$.

Having determined the functions f_2 and f_3 (*see* Figs. 45 and 46), appropriate to profiles on the one hand with high skin friction, and on the other with zero skin friction, it was assumed that approximations to f_2 and f_3 for intermediate profiles might be obtained by interpolating linearly with c. That is to say, for a particular value of c (say c_1), it was assumed that values of f_2 and f_3 for $\eta = \eta_1$ could be found with sufficient accuracy from the following expressions.

$$f_2 = [f_2(\eta_1)]_1 - \{[f_2(\eta_1)]_1 - [f_2(\eta_1)]_2\} \frac{0{\cdot}493 + c_1}{1{\cdot}493}$$

$$f_3 = [f_3(\eta_1)]_1 - \{[f_3(\eta_1)]_1 - [f_3(\eta_1)]_2\} \frac{0{\cdot}493 + c_1}{1{\cdot}493} .$$

The process of interpolation was carried out graphically, as shown in the diagram, for values of $\eta_1 = 0{\cdot}1, 0{\cdot}2, 0{\cdot}3 \ldots 0{\cdot}9$.

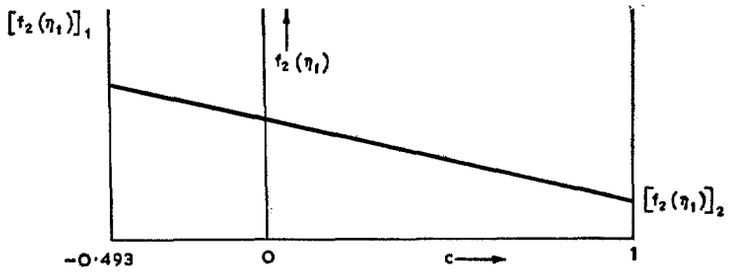

A family of approximate profiles was then built up by giving c a series of values, for each of which f_2 and f_3 were determined as described above, and d given various values, from which the profiles followed.

As might be expected, for a given value of c only a limited range of d gave profiles which appeared physically acceptable. As well as the limitation that u/U must not exceed unity, it was further assumed that for $1/U\ (\partial^2 u/\partial\eta^2)_0 > 0$, $1/U\ \partial^2 u/\partial\eta^2$ must be positive for all values of η*.

4.5. *Calculation of Characteristic Quantities.*—For the family of velocity profiles built up by the method of the previous sections it was first necessary to determine the quantities θ, δ*, ε and

$$\int_0^1 \frac{1}{U^2} \left(\frac{\partial u}{\partial \eta}\right)^2 \partial\eta .$$

The first three presented little difficulty, but for the last it was necessary to know $1/U\ \partial u/\partial\eta$ through the boundary layer. Since

$$\frac{1}{U}\frac{\partial u}{\partial \eta} = f' = f_1' + cf_2' + df_3' ,$$

$[f_2]_1$, $[f_2]_2$, $[f_3]_1$ and $[f_3]_2$ were differentiated graphically so that by linear interpolation the values of f_2' and f_3' corresponding to any given value of c could be found. Since f_1' was known from an exact solution, values of f' readily followed. The functions f_1', f_2' and f_3' are shown in Figs. 47 and 48.

Simpson's Rule was used to integrate $1 - u/U$, $u/U(1 - u/U)$, $u/U[1 - (u/U)^2]$ and $[1/U\ \partial u/\partial\eta]^2$ through the boundary layer. When these quantities had been determined, θ was taken as the characteristic length and values of H_ε, H, l, m and D* calculated. H_ε, H and D* were then plotted as functions of l and m. Further, values of y/θ for given values of u/U could be plotted in the same way, thus enabling the velocity profiles corresponding to given values of l and m to be quickly obtained. A large number of comparisons between known profiles and points obtained from these curves have been made and in all cases the agreement is extremely satisfactory; for lack of space the comparisons are not given here.

* This latter assumption was probably over-restrictive. When suction is applied to a layer which has advanced a considerable distance towards separation, it seems likely that the skin friction will increase while the inflexion point in the profile will persist for some distance downstream.

4.6. *Further Extension of Range of Profiles.*—With one exception all types of profiles known to the author lie within the range of profiles built up by the method described; the important exception is a small set of similar profiles with suction given by Thwaites[24]. These profiles have a very high skin friction and a large curvature at the surface. Unfortunately, they could not be used to obtain values of f_2 and f_3 which would have extended the range of profiles beyond the asymptotic suction profile, because of the uncertainty of the value of y at $u/U = 0{\cdot}995$. However, it seemed that these profiles were in no way anomalous and that it should be possible to extend the l, m charts to take in the region in which they lay. These profiles indicated further that, with suction, profiles may be obtained which lie far outside the range of profiles covered by solid-boundary problems; the examples treated in Section 10 show that this is in fact the case. To extend the charts, values of y/θ for given values of u/U were first considerably extrapolated. These extrapolations were then used to plot profiles in the extrapolated region and where necessary the values were slightly altered so that smooth profiles were obtained. The values of θ were then calculated for these profiles and where these differed by more than 2 per cent from unity the extrapolated values were again adjusted. The further boundary-layer characteristics H, H_ε and D^* were then calculated for these profiles and plotted on the appropriate charts.

By the above procedure the range of profiles covered by the charts was greatly extended. Figs. 49 to 51 show the full range of profiles for $m \leqslant 0$.

5.6. *Stability of the Laminar Boundary Layer.*—According to the stability theory of Tollmien and Schlichting there exists for any given boundary-layer velocity profile a boundary-layer Reynolds number below which infinitesimal disturbances of all frequencies are damped and above which amplification or disturbances of particular frequencies may take place.

Lin[26] gives a particularly simple formula by which the critical boundary-layer Reynolds number may be calculated, when the velocity profile and its first and second derivatives with respect to y are known. Since velocity profiles are given for the range covered in the charts it should be possible to construct a similar chart on which critical boundary-layer Reynolds number is plotted as a function of l and m. The first derivatives of the profiles had been determined in finding D^*, the dissipation function, so that it was in fact possible to obtain the second derivative by differentiating graphically a second time. The first and second derivatives for profiles with $m \leqslant 0$ are shown in Figs. 52 and 53.

Lin's formula may be written

$$R_{\theta\,\mathrm{crit}} = \frac{25l}{u_c^4},$$

where u_c is the velocity for which the following equation is satisfied:

$$l\left[2l\frac{y}{u} - 3\right]\frac{u(\partial^2 u/\partial y^2)}{(\partial u/\partial y)^3} = 0{\cdot}185\,. \qquad (5)$$

To avoid introducing further notation y is here used for y/θ and u for u/U.

For some twenty profiles the left-hand side of the second expression was calculated and plotted for a series of values of y using Figs. 53 and 54. To achieve the necessary accuracy and consistency of results, values of u close to the surface were obtained by integrating the values of $\partial u/\partial y$ in Fig. 52. It was found that there were in general two values of u which satisfied equation (5). Comparison with known values of $R_{\theta\,\mathrm{crit}}$ for the asymptotic suction profile and the Blasius profile indicated that the smaller values of u and y were in fact appropriate. Fig. 54 shows the graphical solution of equation (5) for one value ot l and three values of m.

The values of $R_{\theta\,\mathrm{crit}}$ found as above were reasonably consistent and in good agreement with accepted values where these were known. Curves of constant $R_{\theta\,\mathrm{crit}}$ plotted as a function of l and m are shown in Fig. 55. Within the region to the right of the dotted line it is believed that the values given will be accurate to within the limits imposed by the approximate nature of Lin's formula.

It has been suggested by Chiarulli and Freeman[27] that $R_{\theta\,\mathrm{crit}}$ may be taken as a unique function of H. For the most commonly occurring profiles this is probably not an unreasonable approximation, since such profiles tend, in the region of negative m, to form a one-parameter family. From the present results, however, it appears that, for the full range of profiles which may be obtained with suitable combinations of suction and pressure gradient, H cannot be considered a suitable criterion of stability. From Fig. 55 it appears that for values of l greater than, say, 0·35, the ratio m/l might be accepted as a more satisfactory criterion.

6. *Distributed Suction Applied to an Aerofoil.*—The case is considered of suction applied to the upper surface of an aerofoil at a positive incidence. The velocity distribution chosen presents a simple example since the pressure is uniform from the leading edge to 40 per cent of the chord. Figs. 56 and 57 show the chordwise distribution of external velocity and velocity gradient, and the four different distributions of suction velocity for which calculations were carried out. Since the suction and external velocities were uniform up to 40 per cent. of the chord, the Iglisch solution for the flat plate could be used to obtain starting values of l, m, and t^* at this point. The results of the calculations are shown in Figs. 58 and 59. It will be seen that a very wide range of velocity profiles is covered; it was not in fact found possible to complete the calculations for the highest rate of suction. With reference to Fig. 59, the critical boundary-layer Reynolds numbers quoted have been obtained from Fig. 56. It is interesting to note that a 30 per cent increase in mean suction velocity at a given chord Reynolds number results in an increase in the critical Reynolds number of the boundary layer at the trailing edge to between twenty and thirty times the initial value. This is of assistance in interpreting previous experimental results. It has always appeared somewhat anomalous that, although it is known that the critical boundary-layer Reynolds number may be very greatly exceeded before transition takes place, yet the suction quantities so far found necessary to preserve laminar flow are not greatly different from those calculated by approximate methods as being necessary to preserve formal stability of the boundary layer. In the light of the present example this is no longer surprising, since small changes in suction velocity evidently result in quite disproportionate changes in boundary-layer stability.

7. *Concluding Remarks.*—The examples treated in Part I show close agreement between results obtained using the present method and the corresponding exact, or nearly exact, solutions. In developing the present method, the only appeal to exact solutions has been in the choice of four known velocity profiles, so that the accuracy with which the standard cases have been treated may be taken as a fair indication of the accuracy which will be achieved in the general case. The method is applicable equally to solid-boundary problems and to problems involving suction, and will be preferred to existing approximate methods wherever additional accuracy is required at the expense of some increase in computing time.

8. *Acknowledgements.*—The author wishes to acknowledge gratefully the assistance of Miss Jean Wilson, who carried out a large part of the computation necessary for the development of the method, and to record his appreciation of helpful correspondence with Mr. E. J. Watson of Liverpool University.

NOTATION

The notation is as far as possible conventional and follows, in the main, that used by Thwaites.

General

x		Distance along surface
y		Distance normal to surface
U_0		Free-stream velocity
U		Velocity at edge of boundary layer
u		Velocity in boundary layer in x direction
u_c		Value of u at critical value of y
v		Velocity in boundary layer in y direction
v_s		Velocity at surface in direction of y negative
δ		Boundary-layer thickness
δ^*		Displacement thickness
	$=$	$\int_0^\delta \left(1 - \frac{u}{U}\right) dy$
θ		Momentum thickness
	$=$	$\int_0^\delta \frac{u}{U}\left(1 - \frac{u}{U}\right) dy$
ε		Energy thickness
	$=$	$\int_0^\delta \frac{u}{U}\left\{1 - \left(\frac{u}{U}\right)^2\right\} dy$
c		Chord, or representative length
ρ		Density
μ		Viscosity
ν		Kinematic viscosity
R_c		Chord Reynolds number
R_x		Reynolds number based on x
R_θ		Reynolds number based on momentum thickness
$R_{\theta\,\mathrm{crit}}$		Critical value of R_θ
$\bar{x}$	$=$	x/c
$\bar{U}$	$=$	U/U_0
D^*		Dissipation integral
	$=$	$\int_0^{\delta/\theta} \left(\frac{\theta}{U}\right)^2 \left(\frac{\partial u}{\partial y}\right)^2 d\left(\frac{y}{\theta}\right)$
H	$=$	δ^*/θ
H_ε	$=$	ε/θ
λ	$=$	$v_s\theta/\nu$

NOTATION—*continued*

$$\Lambda = \frac{\theta^2}{\nu}\frac{dU}{dx}$$

$$l = \frac{\theta}{U}\left(\frac{\partial u}{\partial y}\right)_0$$

$$m = \frac{\theta^2}{U}\left(\frac{\partial^2 u}{\partial y^2}\right)_0$$

Subscript $_0$ refers to values at surface

$$t^* = \left(\frac{\theta}{c}\right)^2 R_c$$

$$v_s^* = \frac{v_s}{U_0}\sqrt{R_c}$$

$$\xi = \left(\frac{v_s}{U_0}\right)^2 R_x$$

$$\eta = y/\delta$$

A_1, A_2, A_3 — Constants used by Wieghardt[2] in polynomial representation of velocity profiles

f_1, f_2, f_3 — Functions of η defined in Sections 4.1 and 4.2

a, b — Constants used by Wieghardt[2] to define approximate profiles in terms of f_1, f_2 and f_3

c, d — Corresponding constants used in present method.

The following additional notation is used in comparing results obtained by the present method with certain exact solutions. The notation is in most cases that of the original authors but certain symbols have been changed to avoid confusion.

Howarth[8]

b_0, b_1 — Constants ($U = b_0 - b_1 x$)

$$\chi = \frac{b_1^{1/2}}{\nu^{1/2}}\theta$$

δ_1 — Displacement thickness

$$\delta_1^* = \frac{b_1^{1/2}}{\nu^{1/2}}\delta_1$$

$$x^* = \frac{b_1^{1/2}}{\nu^{1/2}}x$$

$$\left(\frac{\partial u}{\partial y}\right)_0^* = \frac{\nu^{1/2}}{b_0 b_1^{1/2}}\left(\frac{\partial u}{\partial y}\right)_0$$

$$\zeta = \frac{y}{\theta}\frac{\chi}{2x^{*1/2}}$$

Thwaites[9]

$$h = y\sqrt{\frac{U_0}{\nu x}}$$

σ_1 — Constant ($v_s = \sigma_1 x^{1/2}$)

Schlichting and Bussmann[10]

u_1 Constant ($U = u_1 x$)

$$C_0 = \frac{v_s}{\sqrt{u_1 \nu}}$$

Falkner and Skan[11], and Hartree[12]

C, n Constants ($U = Cx^n$)

$$\beta = \frac{2n}{n+1}$$

$$k = \frac{1-n}{n}$$

$$Y = \frac{y}{x}\left(\frac{Ux}{\nu}\right)^{1/2}\left[\tfrac{1}{2}(n+1)\right]^{1/2}$$

$$\Theta = \frac{\theta}{x}\left(\frac{Ux}{\nu}\right)^{1/2}\left[\tfrac{1}{2}(n+1)\right]^{1/2}$$

$$\Delta^* = \frac{\delta^*}{x}\left(\frac{Ux}{\nu}\right)^{1/2}\left[\tfrac{1}{2}(n+1)\right]^{1/2}$$

REFERENCES

No.	*Author*	*Title, etc.*
1	M. R. Head, D. Johnson and M. Coxon	Flight experiments on boundary-layer control for low drag. R. & M. 3025. March, 1955.
2	K. Wieghardt	On an energy equation for the calculation of laminar boundary layers. Reports and Translations No. 89 (MAP–VG109–89T); also *Ing.-Arch.* 16. p. 231. 1948.
3	K. Pohlhausen	On the approximate integration of the differential equation of the laminar boundary layer. *Z.A.M.M.* Vol 1. p. 252. 1921.
4	H. Schlichting	An approximate method for the calculation of the laminar boundary layer with suction for bodies of arbitrary shape. N.A.C.A. Tech. Memo. 1216. 1949.
5	E. Truckenbrodt	A simple approximate method for calculating the laminar boundary layer with suction. Report No. 55/6a. Institut für Strömungsmechanic, Technische Hochschule, Braunschweig. 1955.
6	A. Walz	Application of the energy equation by K. Wieghardt on one-parametric velocity profiles in laminar boundary layers. *Ing. Arch.* 16. p. 243. 1948.
7	K. Wieghardt	On the calculation of plane and axisymmetric boundary layers with continuous suction. *Ing.-Arch.* 22. pp. 368 to 377. 1954.
8	L. Howarth	On the solution of the laminar boundary-layer equations. *Proc. Roy. Soc.* 164. pp. 547 to 578. 1938.
9	B. Thwaites	An exact solution of the boundary-layer equations under particular conditions of porous suction. R. & M. 2241. May, 1946.
10	H. Schlichting and K. Bussmann	Exact solutions for the laminar boundary layer with suction and blowing. *Schr. der Deut. Akad. der Luft.* May, 1943.
11	V. M. Falkner and S. W. Skan ..	Some approximate solutions of the boundary-layer equations. R. & M. 1314. 1930.
12	D. R. Hartree	On an equation occurring in Falkner and Skan's approximate treatment of the equations of the boundary layer. *Proc. Camb. Phil. Soc.* Vol. 33. pp. 223 to 239. 1937.
13	G. B. Schubauer	Airflow in a separating laminar boundary layer. N.A.C.A. Report 527. 1935.
14	D. R. Hartree	A solution of the boundary-layer equation for Schubauer's observed pressure distribution on an elliptic cylinder. R. & M. 2427. April, 1939.
15	K. Hiemenz	On the boundary layer of a circular cylinder immersed in the steady flow of fluids. *Dingler's Polytechn. Journal.* Vol. 326. p. 321. 1911.
16	H. Görtler	Further development of a boundary-layer profile for a given pressure distribution. *Z.A.M.M.* Vol. 19. pp. 129 to 140. 1939.
17	H. Görtler	A method of differences for the calculation of laminar boundary layers. Untersuchungen u. Mitteilungen No. 6615, 1944; also *Ing.-Arch.* 16. p. 173. 1948.
18	B. Thwaites	Approximate calculations of the laminar boundary layer. *Aero. Quart.* Vol. 1. p. 245. 1949.
19	R. Iglisch	Exact calculation of the laminar boundary layer in longitudinal flow over a flat plate with homogeneous suction. N.A.C.A. Tech. Memo. 1205. 1949.
20	E. J. Watson	Private communication. 1949.

REFERENCES—*continued.*

No.	*Author*	*Title, etc.*
21	H. Schlichting	The boundary layer of a flat plate under conditions of suction and air ejection. R.T.P. Trans. 1753. A.R.C. 6634. 1946.
22	J. H. Preston	The boundary layer over a permeable surface through which suction is applied. R. & M. 2244. February, 1946.
23	A. Betz (General Editor) ..	A. V. A. Monographs. Reports and Translations No. 1001 (MAP–VG 301–T). 1948.
24	B. Thwaites	The development of laminar boundary layers under conditions of continuous suction. (Part II) A.R.C. 12,699. November, 1949.
25	A. Betz (General Editor) ..	A. V. A. Monographs. Reports and Translations No. 1002. (MAP–VG 302–T). p. 47. 1948.
26	C. C. Lin	On the stability of two-dimensional parallel flows. *Quart. J. App. Math.* Vol. 3. 1945.
27	P. Chiarulli and J. C. Freeman ..	Stability of the boundary layer. Technical Report F–TR–1197–IA. Wright-Patterson Air Force Base. August, 1948.

APPENDIX

Derivation of Equations used in Present Method

(i) Momentum Equation.

For two-dimensional incompressible flow the boundary-layer equation may be written

$$u\frac{\partial u}{\partial x}+v\frac{\partial u}{\partial y}=U\frac{dU}{dx}+\nu\frac{\partial^2 u}{\partial y^2}, \qquad (1)$$

and the equation of continuity

$$\frac{\partial u}{\partial x}+\frac{\partial v}{\partial y}=0. \qquad (2)$$

Multiplying the left-hand side of (2) by u and adding to the left-hand side of (1) we have

$$2u\frac{\partial u}{\partial x}+\frac{\partial}{\partial y}(uv)=U\frac{dU}{dx}+\nu\frac{\partial^2 u}{\partial y^2}.$$

Integrating over y from $y=0$ to $y=h$, where h is a distance greater than the boundary layer thickness and independent of x, we find

$$\int_0^h 2u\frac{\partial u}{\partial x}\,dy+[uv]_0^h=\int_0^h U\frac{dU}{dx}\,dy+\nu\left[\frac{\partial u}{\partial y}\right]_0^h,$$

or

$$\int_0^h 2u\frac{\partial u}{\partial x}\,dy+U\left[\int_0^h\frac{\partial v}{\partial y}\,dy-v_s\right]=\int_0^h U\frac{dU}{dx}\,dy+\nu\left[\frac{\partial u}{\partial y}\right]_0^h,$$

where v_s, the suction velocity, $=-v_0$.

Hence $$\frac{d}{dx}\int_0^h(U^2-u^2)\,dy-U\frac{d}{dx}\int_0^h(U-u)\,dy+v_sU=\nu\left(\frac{\partial u}{\partial y}\right)_0.$$

In the usual notation this becomes

$$\frac{d}{dx}[U^2(\theta+\delta^*)]-U\frac{d}{dx}(U\theta)+v_sU=\nu\left(\frac{\partial u}{\partial y}\right)_0,$$

which upon further simplification reduces to

$$\frac{d\theta}{dx}=\frac{\nu}{U^2}\left(\frac{\partial u}{\partial y}\right)_0-(H+2)\frac{\theta}{U}\frac{dU}{dx}-\frac{v_s}{U}.$$

This may be written

$$\frac{1}{2}\frac{U}{\nu}\frac{d\theta^2}{dx}=\frac{\theta}{U}\left(\frac{\partial u}{\partial y}\right)_0+(H+2)\frac{dU}{dx}\frac{\theta^2}{\nu}-\frac{v_s\theta}{\nu}. \qquad (3)$$

Introducing the notation

$$t^*=\left(\frac{\theta}{c}\right)^2R_c,$$

$$\bar{U}=\frac{U}{U_0},$$

$$l=\frac{\theta}{U}\left(\frac{\partial u}{\partial y}\right)_0,$$

$$\Lambda=\frac{\theta^2}{\nu}\frac{dU}{dx},$$

and

$$\lambda=\frac{\theta v_s}{\nu},$$

equation (3) becomes

$$t^{*\prime}=\frac{2}{\bar{U}}\{l-\Lambda(H+2)-\lambda\},$$

where the prime denotes differentiation with respect to $\bar{x}(=x/c)$.

(ii) Energy Equation.

As before,

$$u\frac{\partial u}{\partial x}+v\frac{\partial u}{\partial y}=U\frac{dU}{dx}+\nu\frac{\partial^2 u}{\partial y^2} \quad .. \quad .. \quad .. \quad .. \quad (1)$$

and

$$\frac{\partial u}{\partial x}+\frac{\partial v}{\partial y}=0 \quad .. \quad .. \quad .. \quad .. \quad .. \quad .. \quad (2)$$

If we add $u/2\,(\partial u/\partial x+\partial v/\partial y)$ to the left-hand side of (1), multiply through by u, and integrate from $y=0$ to $y=h$, we have

$$\int_0^h \frac{3}{2}u^2\frac{\partial u}{\partial x}dy+\int_0^h uv\frac{\partial u}{\partial y}dy+\int_0^h \frac{1}{2}u^2\frac{\partial v}{\partial y}dy-U\int_0^h u\frac{dU}{dx}dy$$
$$=\nu\int_0^h u\frac{\partial^2 u}{\partial y^2}dy\,,$$

i.e., $$\frac{d}{dx}\int_0^h\left(\frac{1}{2}u^3-\frac{1}{2}uU^2\right)dy+\frac{1}{2}\int_0^h U^2\frac{\partial u}{\partial x}dy+\frac{1}{2}[u^2v]_0^h$$
$$=\left[\nu u\frac{\partial u}{\partial y}\right]_0^h-\nu\int_0^h\left(\frac{\partial u}{\partial y}\right)^2dy\,,$$

or $$-\frac{d}{dx}\int_0^h\frac{1}{2}u(U^2-u^2)\,dy+\frac{1}{2}U^2\int_0^h\frac{\partial u}{\partial x}dy+\frac{1}{2}U^2\left[\int_0^h\frac{\partial v}{\partial y}dy-v_s\right]$$
$$=-\nu\int_0^h\left(\frac{\partial u}{\partial y}\right)^2dy\,.$$

Hence $$\frac{1}{2}\frac{d}{dx}\left\{U^3\int_0^h\frac{u}{U}\left[1-\left(\frac{u}{U}\right)^2\right]dy\right\}+\tfrac{1}{2}v_sU^2$$
$$=\nu\int_0^h\left(\frac{\partial u}{\partial y}\right)^2dy\,,$$

or $$\frac{d}{dx}(U^3\varepsilon)=2\nu\int_0^h\left(\frac{\partial u}{\partial y}\right)^2dy-v_sU^2\,, \quad .. \quad .. \quad .. \quad (4)$$

where ε, the energy thickness, $$=\int_0^h\frac{u}{U}\left[1-\left(\frac{u}{U}\right)^2\right]dy\,.$$

This is the energy equation in its usual form.

Now $$\frac{d}{dx}\left(\frac{\varepsilon}{\theta}\right)=\frac{1}{\theta}\frac{d\varepsilon}{dx}-\frac{\varepsilon}{\theta^2}\frac{d\theta}{dx}\,,$$

so that $$\frac{d\varepsilon}{dx}=\theta\frac{dH_\varepsilon}{dx}+H_\varepsilon\frac{d\theta}{dx}\,, \quad .. \quad .. \quad .. \quad .. \quad (5)$$

where $$H_\varepsilon=\frac{\varepsilon}{\theta}\,.$$

Also $$\frac{d}{dx}(U^3\varepsilon)=3U^2\varepsilon\frac{dU}{dx}+U^3\frac{d\varepsilon}{dx}\,,$$

which from (5) becomes

$$\frac{d}{dx}(U^3\varepsilon)=3U^2\varepsilon\frac{dU}{dx}+U^3\theta\frac{dH_\varepsilon}{dx}+U^3H_\varepsilon\frac{d\theta}{dx}\,.$$

Substituting for $d/dx(U^3\varepsilon)$ in (4) we have

$$3U^2\varepsilon\frac{dU}{dx}+U^3\theta\frac{dH_\varepsilon}{dx}+U^3H_\varepsilon\frac{d\theta}{dx}+v_sU^2=2\nu\int_0^h\left(\frac{\partial u}{\partial y}\right)^2dy\,.$$

Substituting for $d\theta/dx$ from (3) and re-arranging, we find

$$\frac{U\theta^2}{\nu}\frac{dH_\varepsilon}{dx}=2\frac{\theta}{U^2}\int_0^h\left(\frac{\partial u}{\partial y}\right)^2dy-H_\varepsilon\left[\frac{\theta}{U}\left(\frac{\partial u}{dy}\right)_0-(H-1)\frac{\theta^2}{\nu}\frac{dU}{dx}-\frac{v_s\theta}{\nu}\right]-\frac{v_s\theta}{\nu}\,,$$

which may be re-written

$$H_\varepsilon'=\frac{1}{\bar{U}t^*}\left[2D^*-H_\varepsilon\{l-\Lambda(H-1)-\lambda\}-\lambda\right],$$

where

$$D^*=\int_0^{h/\theta}\left(\frac{\theta}{\bar{U}}\right)^2\left(\frac{\partial u}{\partial y}\right)^2d\left(\frac{y}{\theta}\right),$$

and the other symbols are as defined above, the prime denoting as before differentiation with respect to $\bar{x}\ (=x/c)$.

(iii) Boundary-Layer Equation at the Surface.

At the surface, $v=-v_s$, $u=0$ and $\partial u/\partial x=0$. Hence the boundary-layer equation for two-dimensional incompressible flow becomes

$$-v_s\left(\frac{\partial u}{\partial y}\right)_0=U\frac{dU}{dx}+\nu\left(\frac{\partial^2u}{\partial y^2}\right)_0,$$

where the subscript $_0$ refers, as elsewhere, to conditions at the surface. Multiplying through by $\theta^2/U\nu$ this becomes

$$-\frac{v_s\theta}{\nu}\frac{\theta}{U}\left(\frac{\partial u}{\partial y}\right)_0=\frac{\theta^2}{\nu}\frac{dU}{dx}+\frac{\theta^2}{U}\left(\frac{\partial^2u}{\partial y^2}\right)_0,$$

which may be written $\quad -\lambda l=\Lambda+m\,,$

or $\quad m=-(\Lambda+l\lambda)\,,$

where $\quad m=\dfrac{\theta^2}{U}\left(\dfrac{\partial^2u}{\partial y^2}\right)_0.$

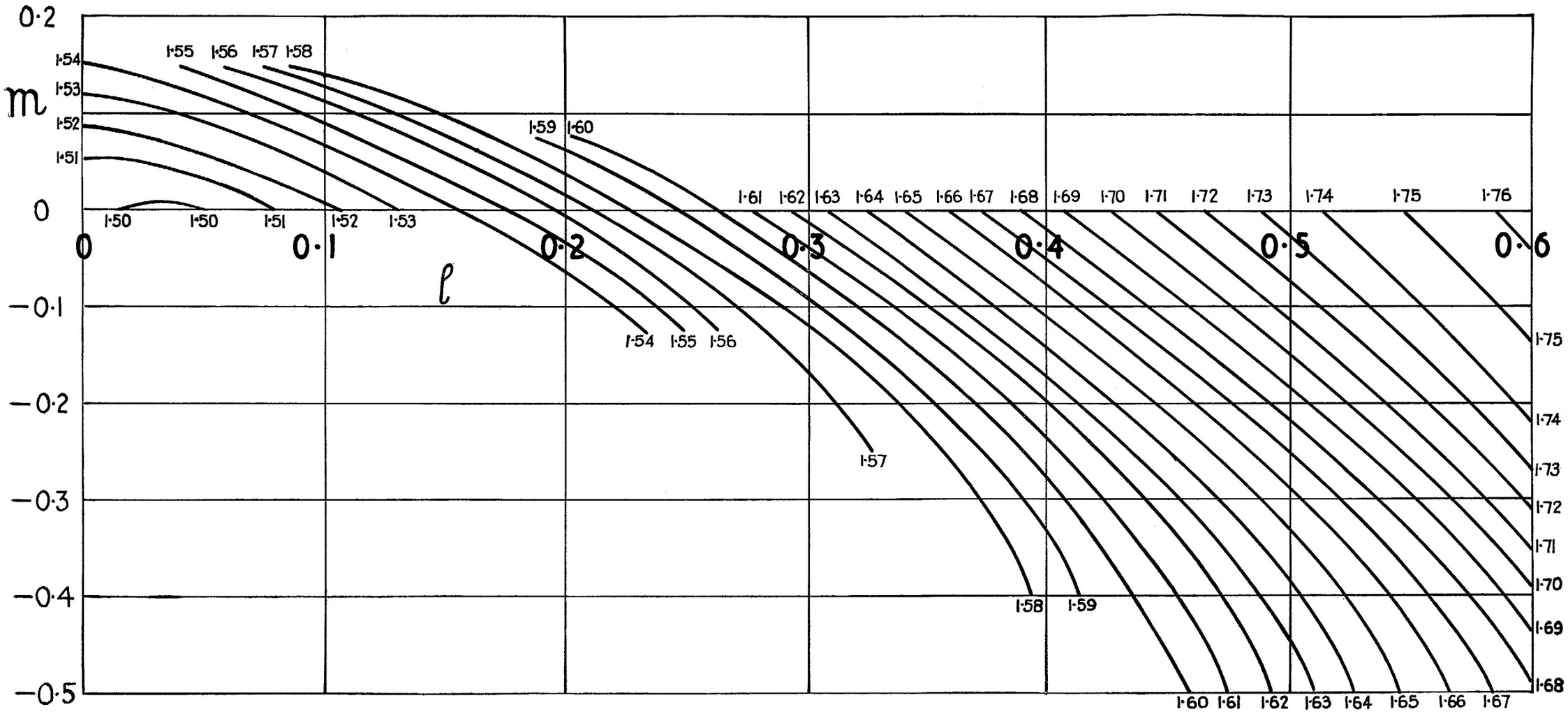

FIG. 1. Variation of H_s with l and m.

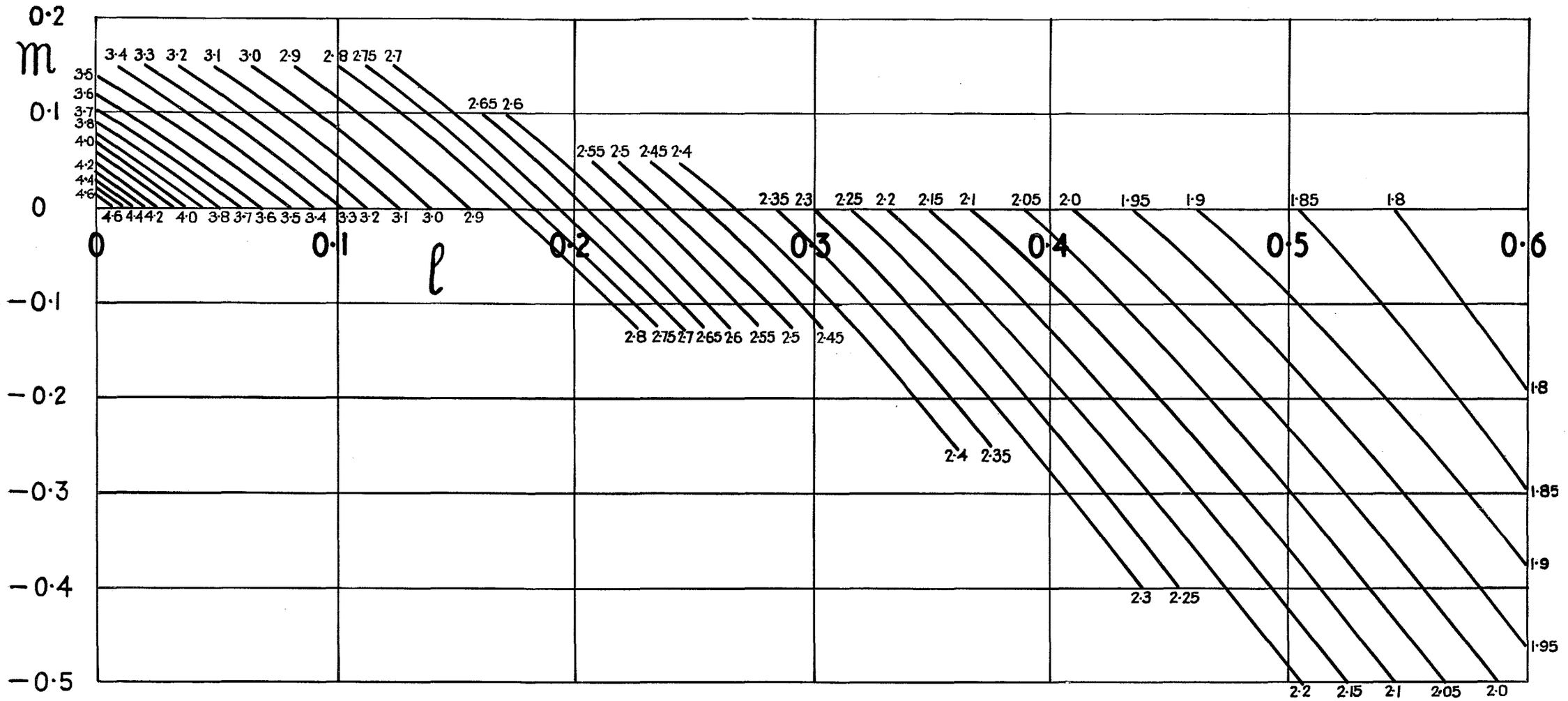

FIG. 2. Variation of H with l and m.

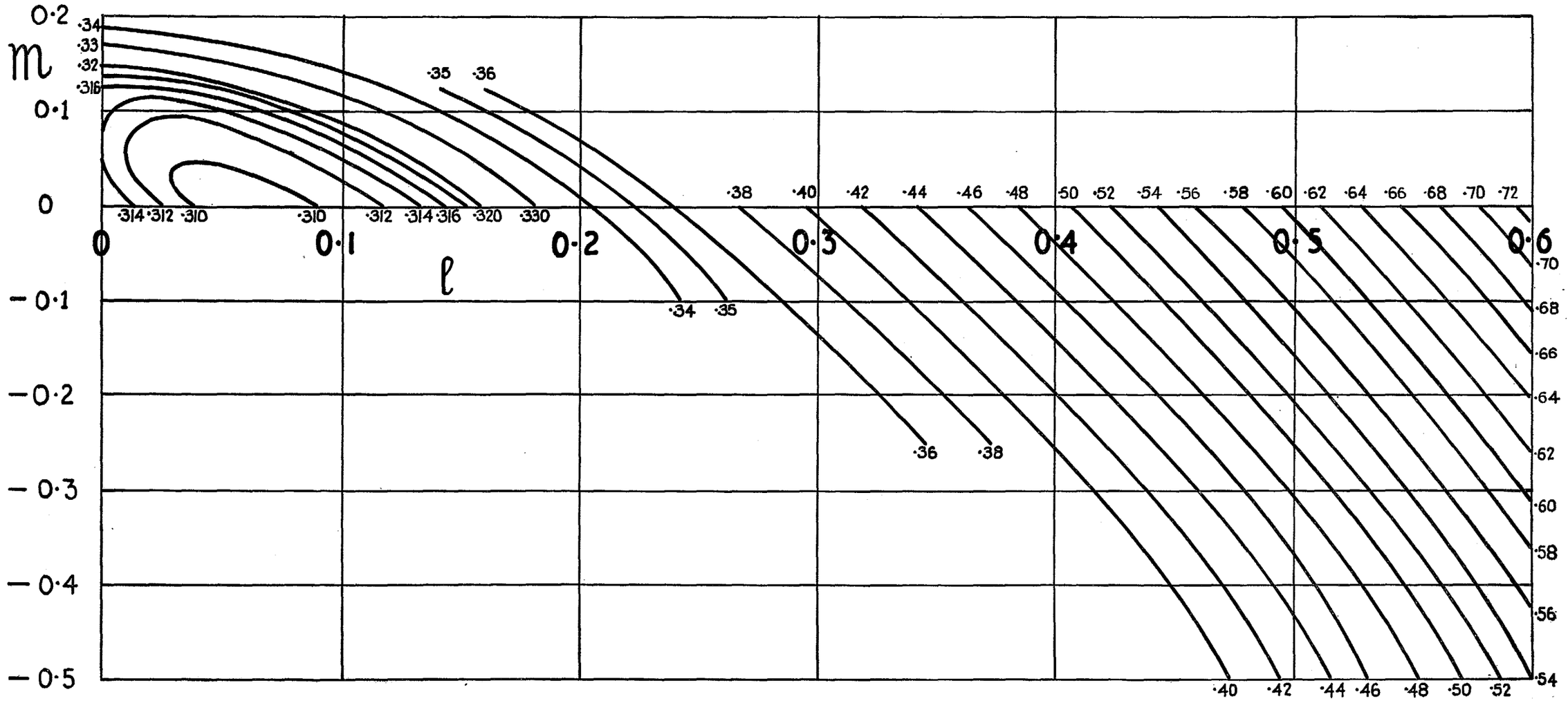

FIG. 3. Variation of $2D^*$ with l and m.

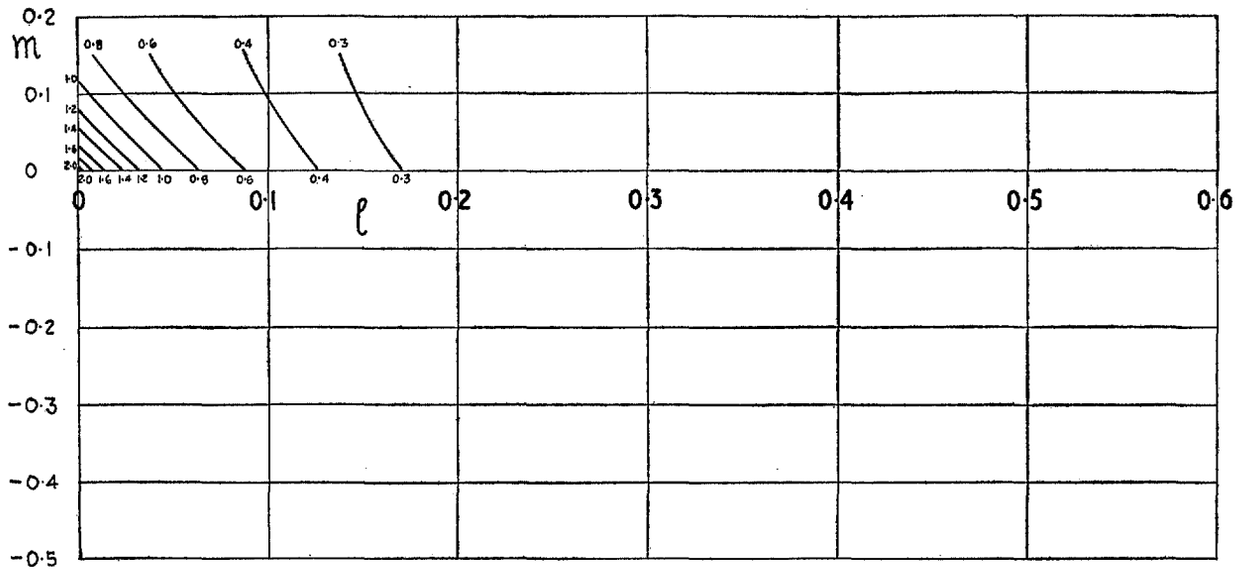

FIG. 4. Variation of y/θ ($u/U = 0{\cdot}05$) with l and m.

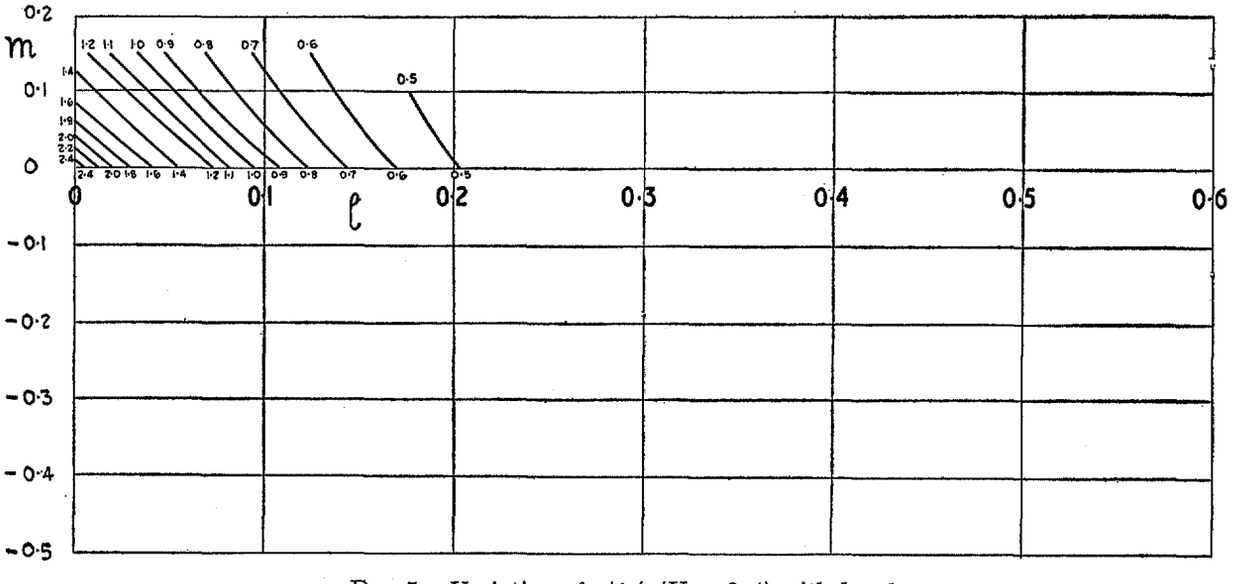

FIG. 5. Variation of y/θ ($u/U = 0{\cdot}1$) with l and m.

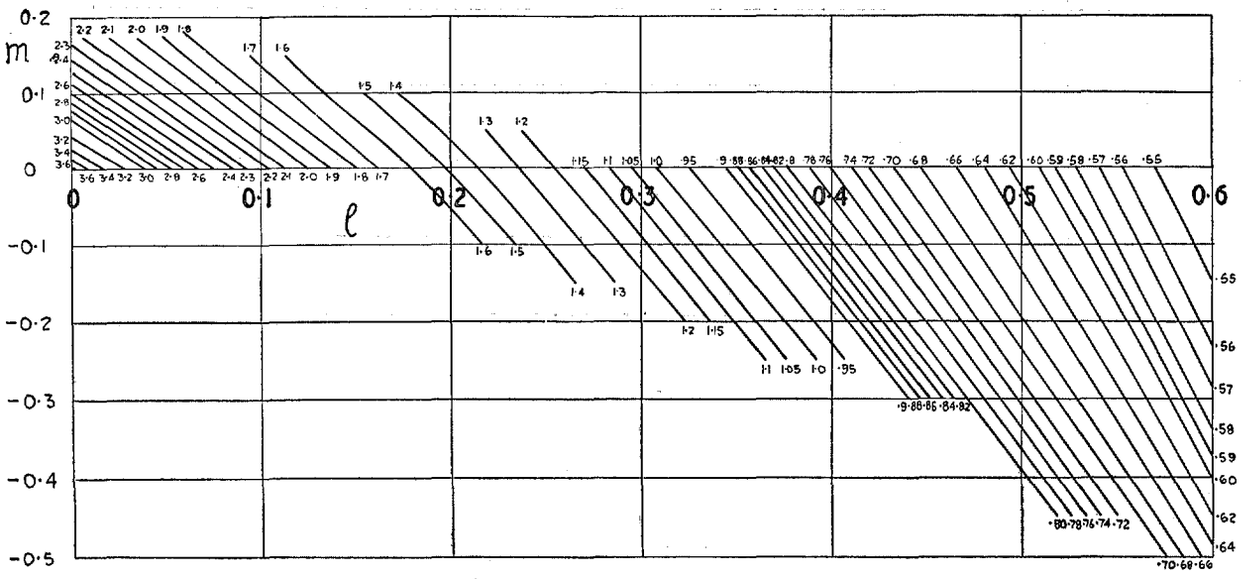

FIG. 6. Variation of y/θ $(u/U = 0{\cdot}3)$ with l and m.

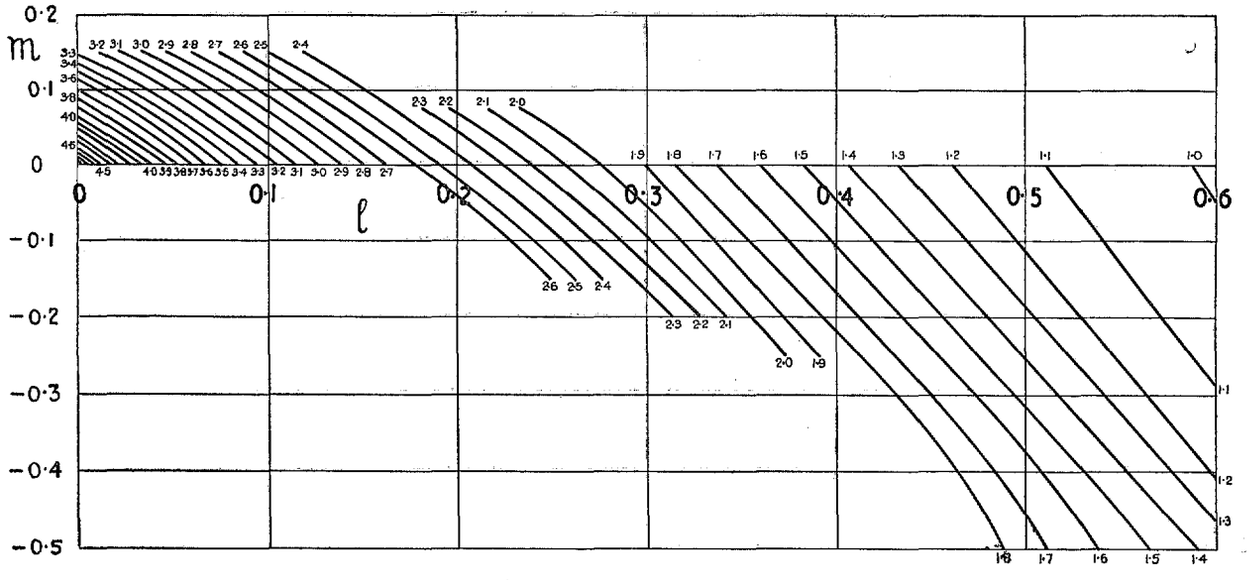

FIG. 7. Variation of y/θ $(u/U = 0{\cdot}5)$ with l and m.

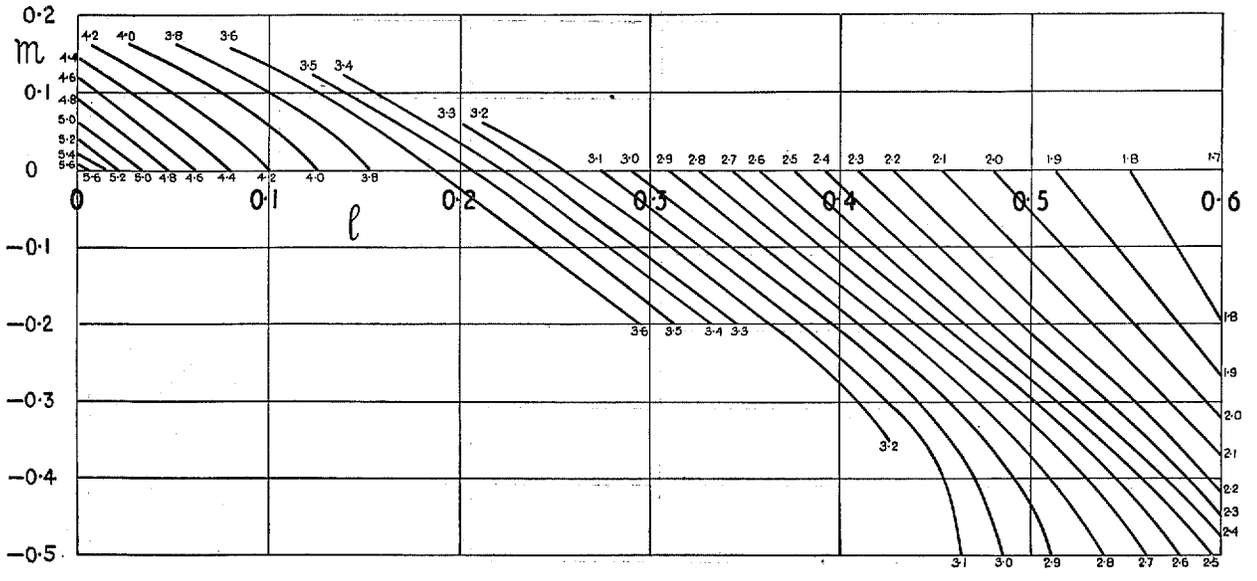

FIG. 8. Variation of y/θ ($u/U = 0{\cdot}7$) with l and m.

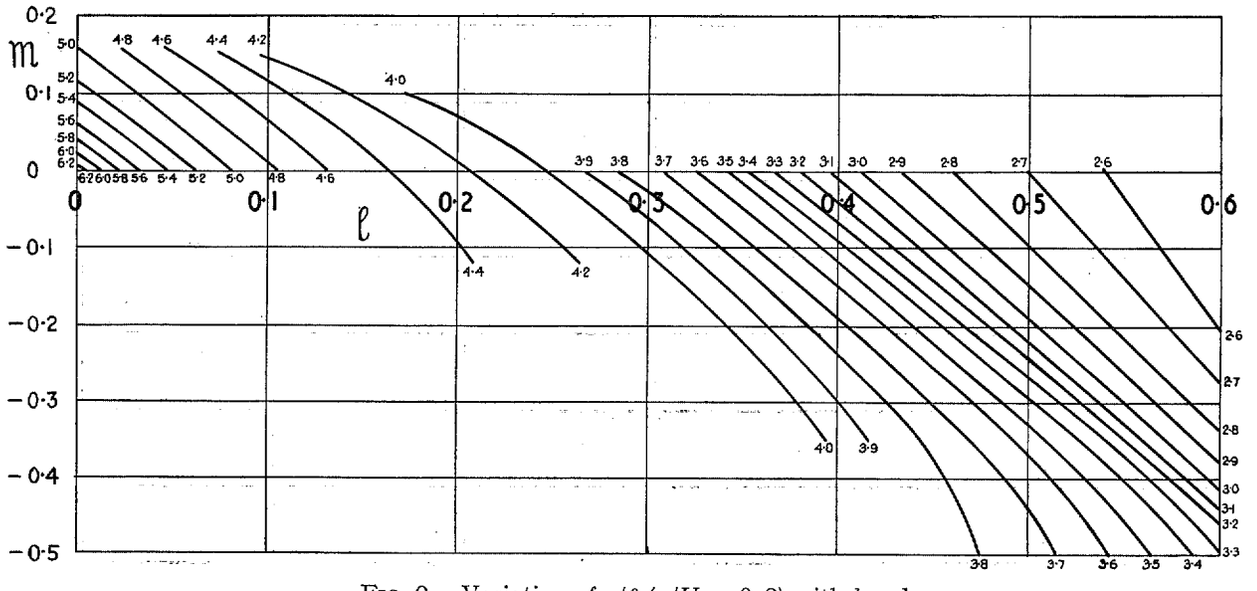

FIG. 9. Variation of y/θ ($u/U = 0{\cdot}8$) with l and m.

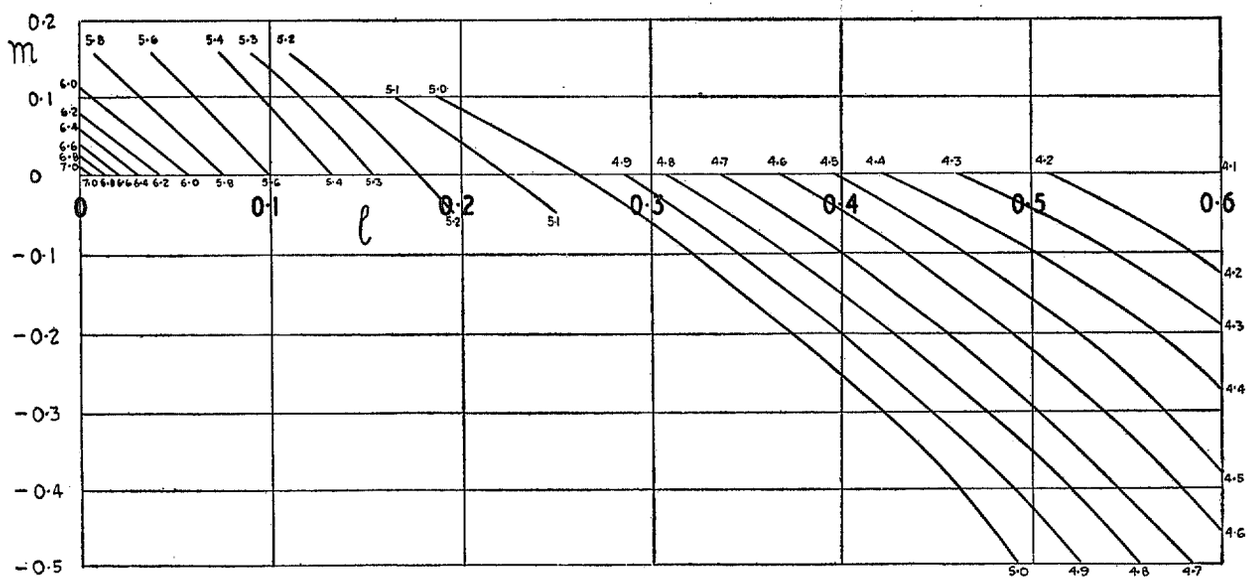

FIG. 10. Variation of y/θ ($u/U = 0{\cdot}9$) with l and m.

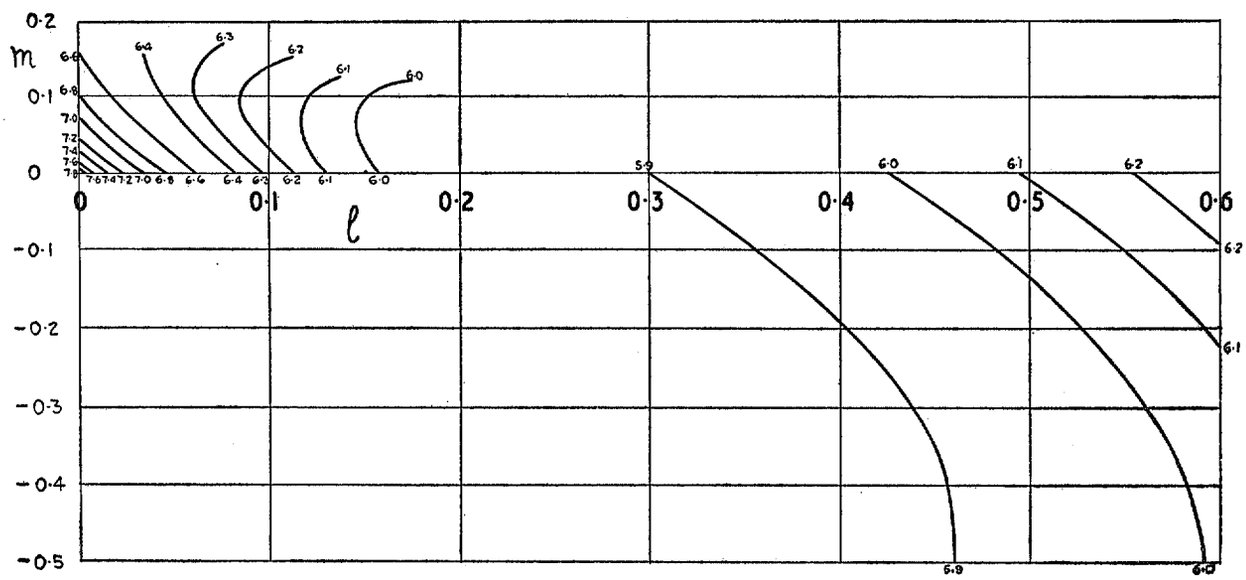

FIG. 11. Variation of y/θ ($u/U = 0{\cdot}95$) with l and m.

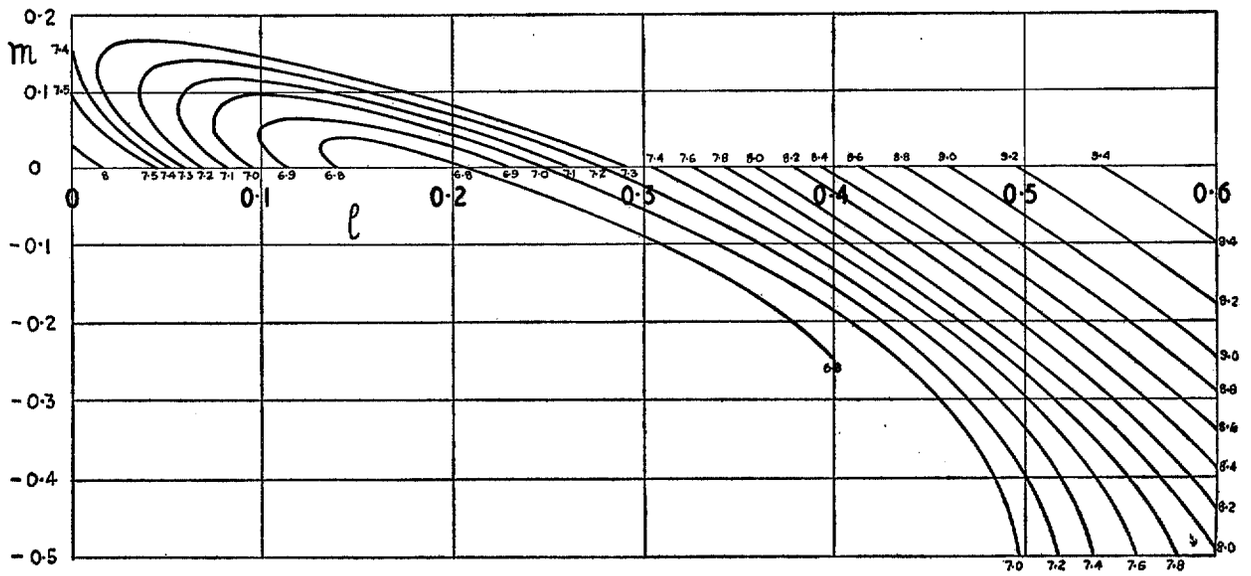

FIG. 12. Variation of y/θ ($u/U = 0{\cdot}98$) with l and m.

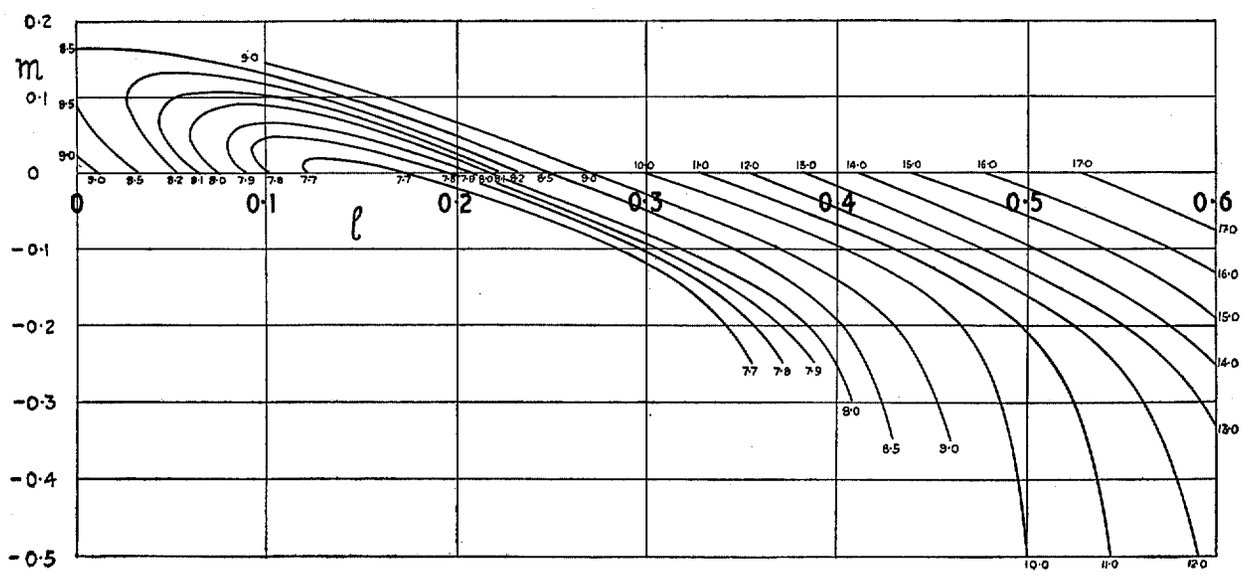

FIG. 13. Variation of y/θ ($u/U = 0{\cdot}995$) with l and m.

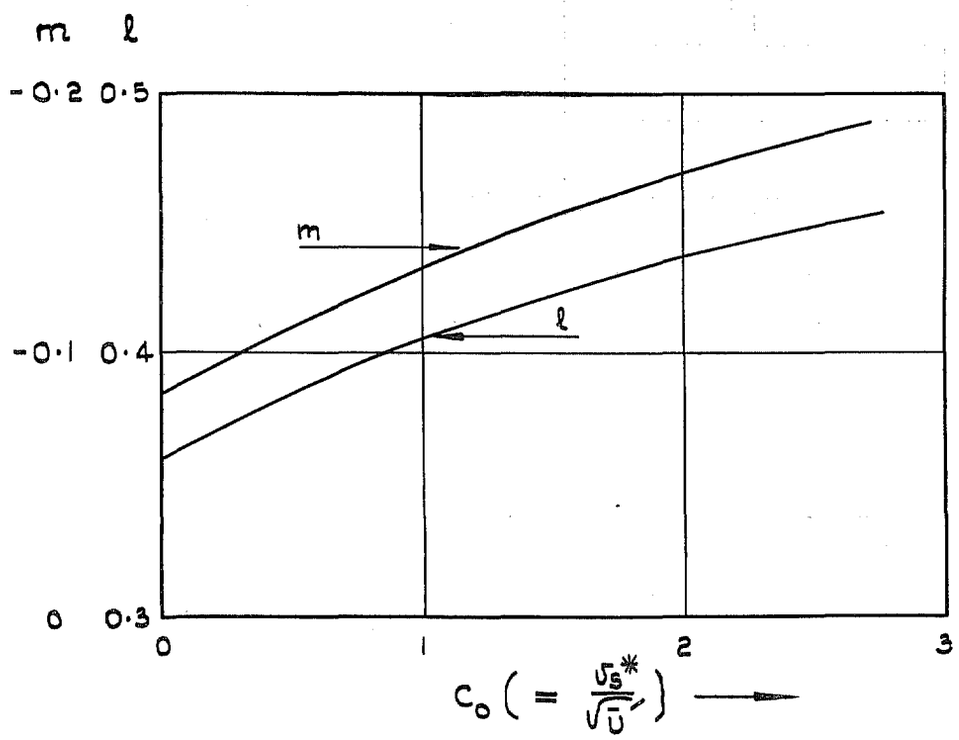

FIG. 14. Stagnation values of l and m given by Schlichting and Bussmann.

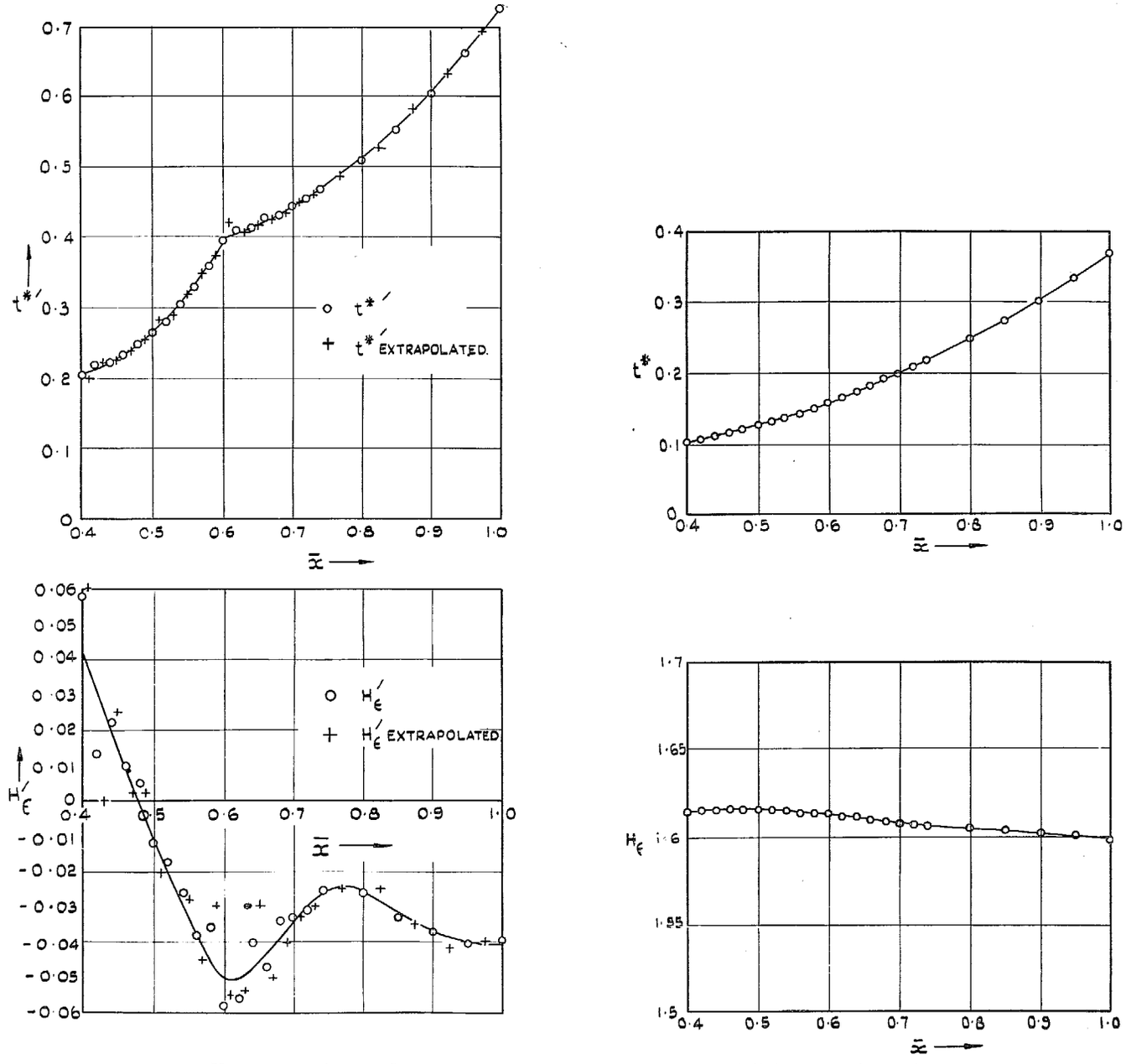

FIGS. 15 and 16. Calculations for upper surface of aerofoil ($0{\cdot}4 < x/c < 1$).

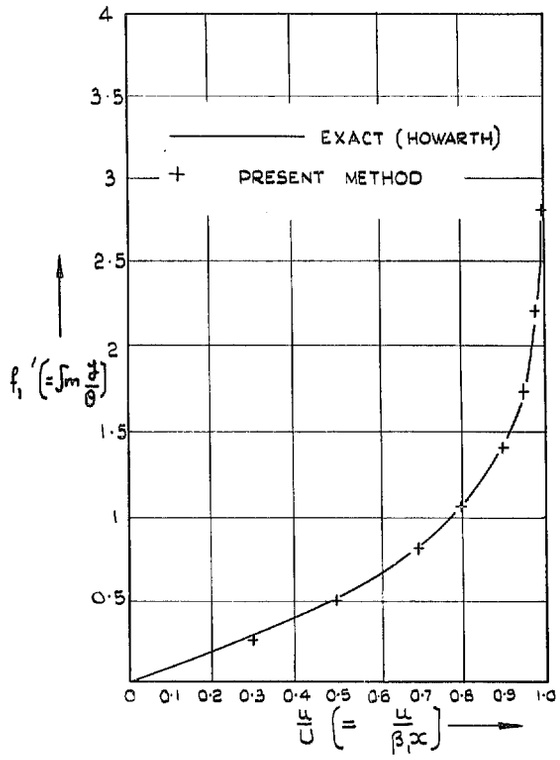

FIG. 17. Stagnation-point profile $U = \beta_1 x$.

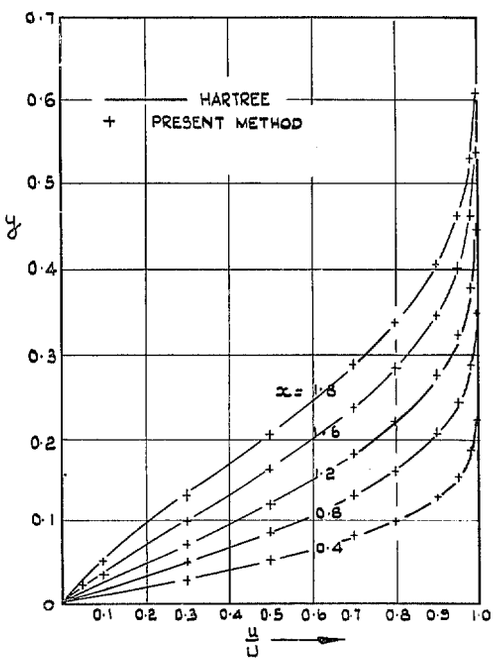

FIG. 18. Boundary-layer velocity profiles for Schubauer's Ellipse.

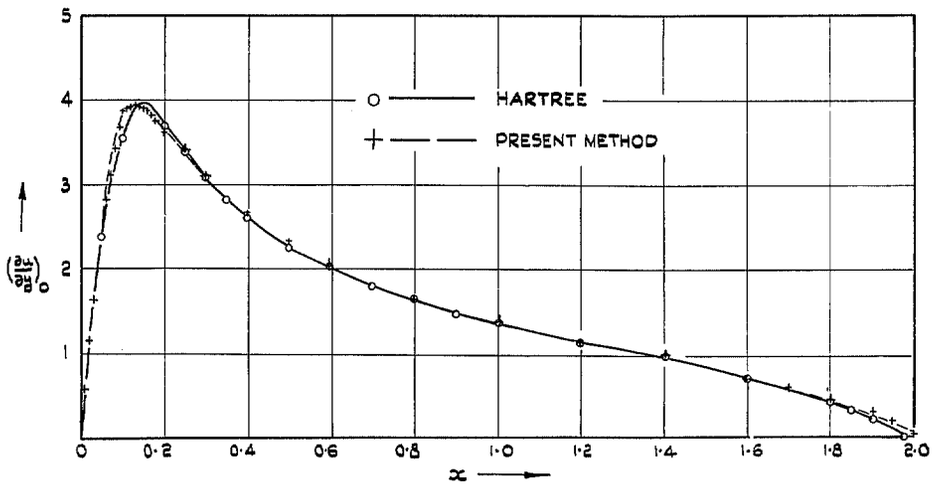

FIG. 19. Distribution of skin friction for Schubauer's ellipse.

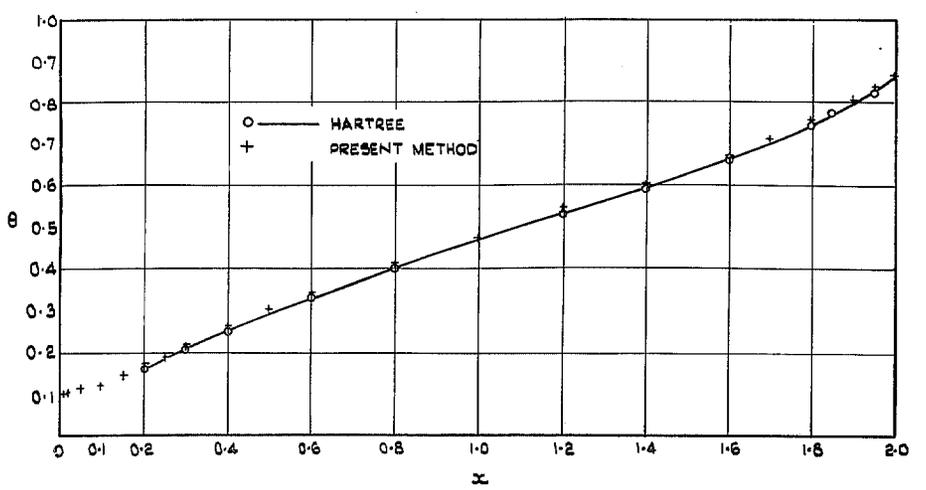

FIG. 20. Growth of momentum thickness.—Schubauer's ellipse.

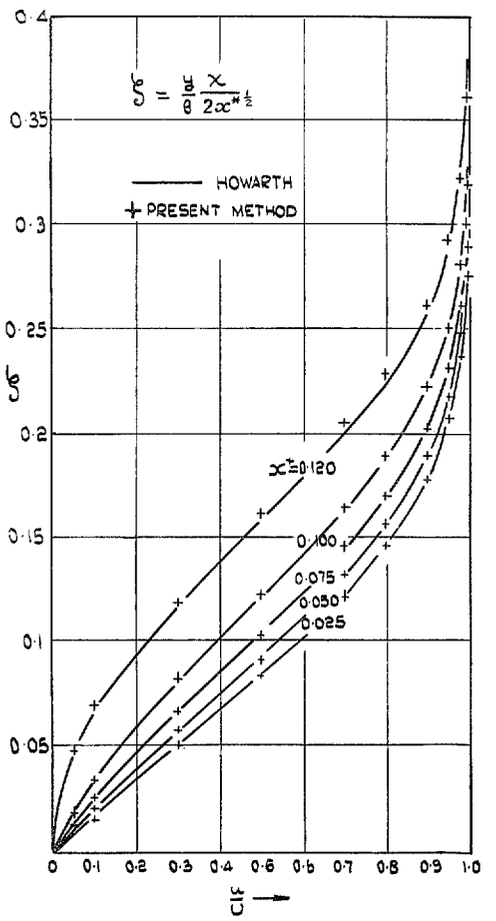

FIG. 21. Boundary-layer velocity profiles for flow $U = b_0 - b_1 x$.

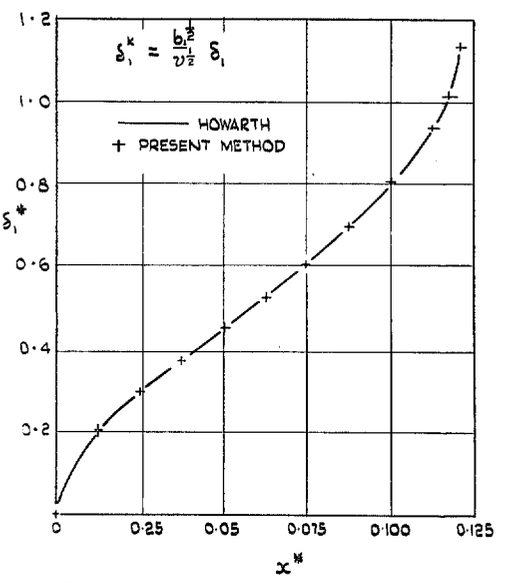

FIG. 22. Growth of displacement thickness for flow $U = b_0 - b_1 x$.

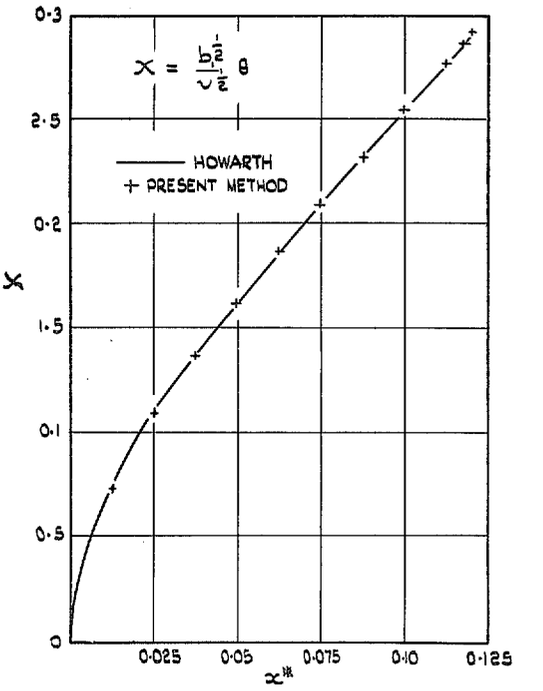

FIG. 23. Growth of momentum thickness for flow $U = b_0 - b_1 x$.

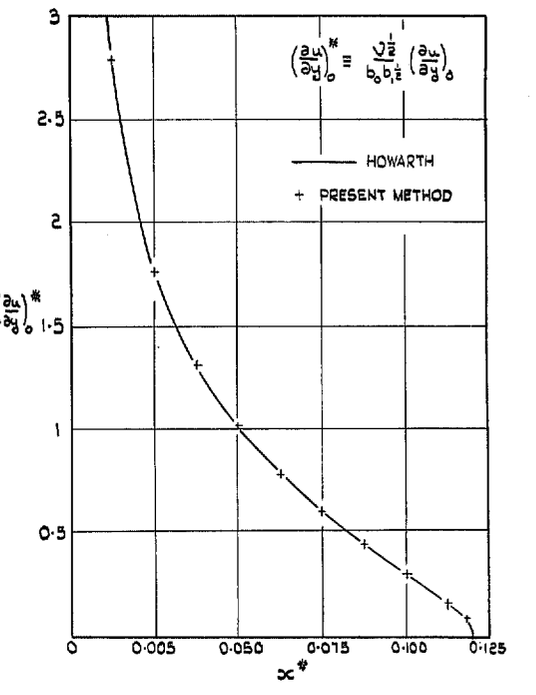

FIG. 24. Variation of skin friction for flow $U = b_0 - b_1 x$.

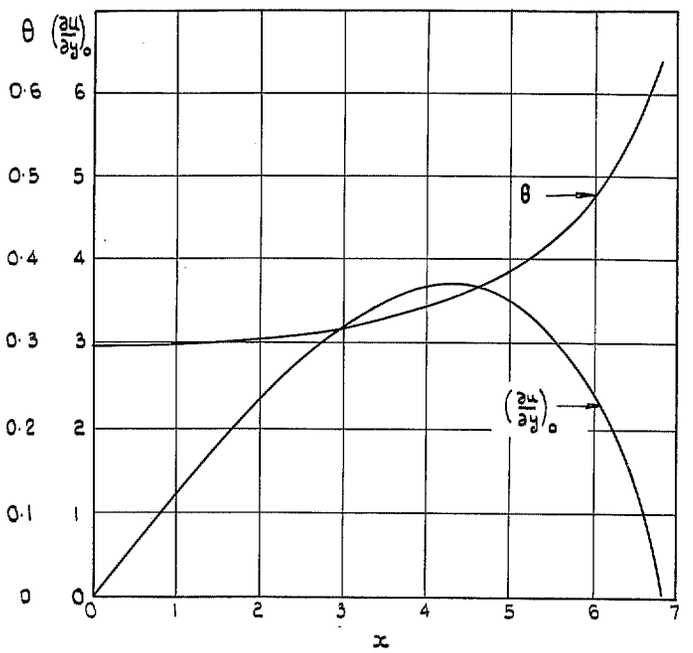

FIG. 25. Development of boundary layer on circular cylinder by present approximate method.

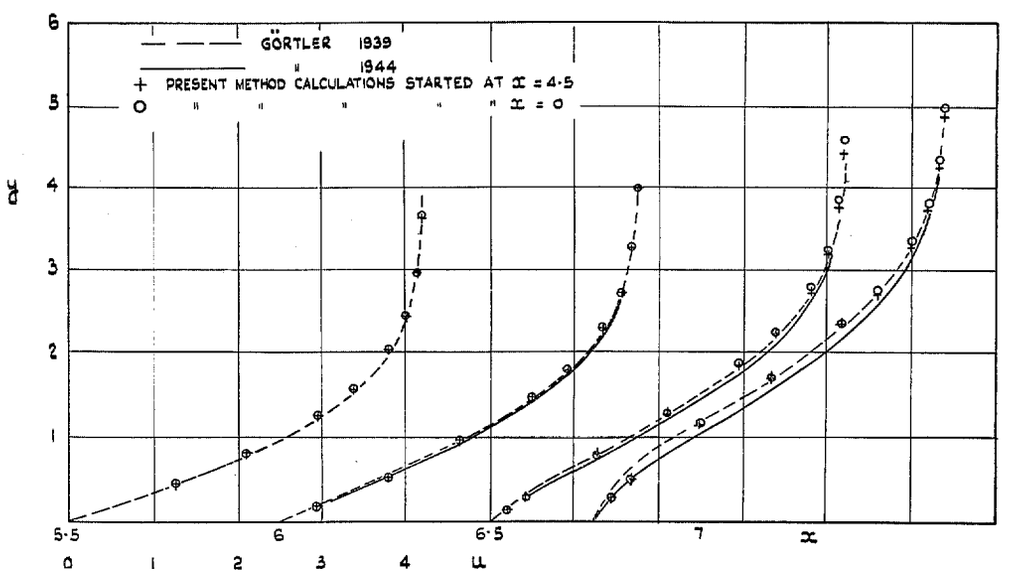

FIG. 26. Velocity profiles for circular cylinder.—Comparison with solutions by Görtler.

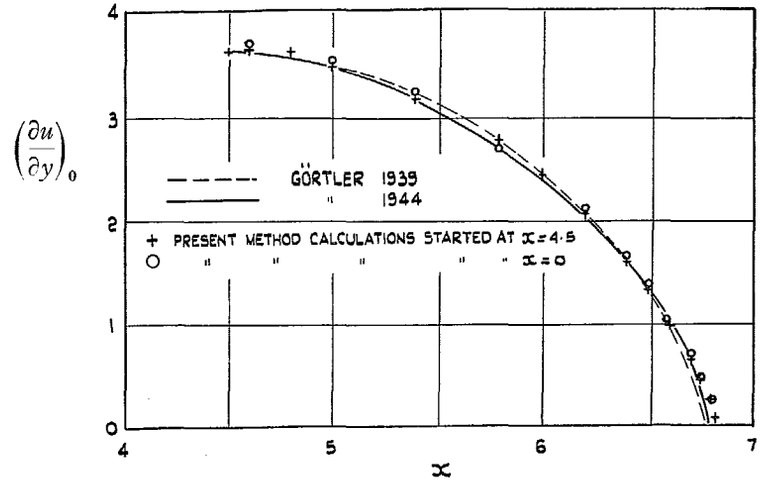

FIG. 27. Skin friction on circular cylinder.—Comparison with solutions by Görtler.

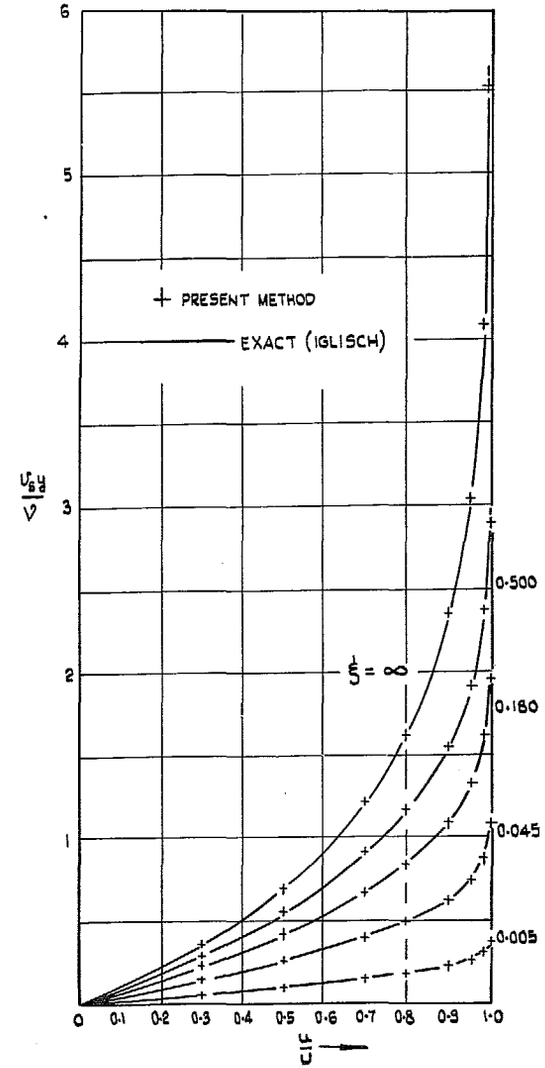

FIG. 28. Boundary-layer velocity profiles for flat plate with uniform suction.

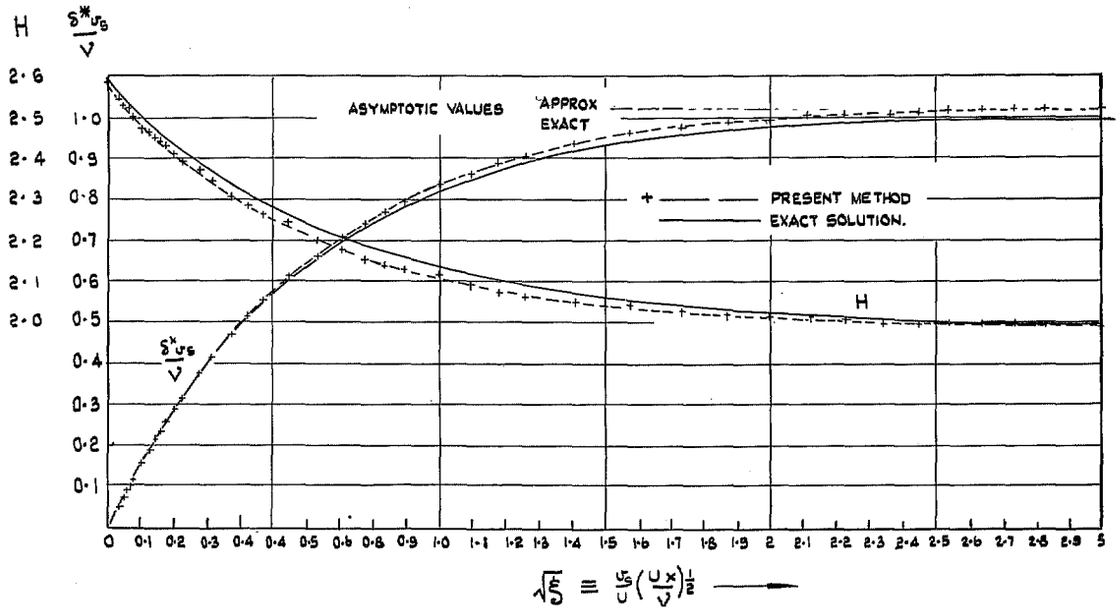

FIG. 29. Variation of displacement thickness and form parameter along flat plate with uniform suction.

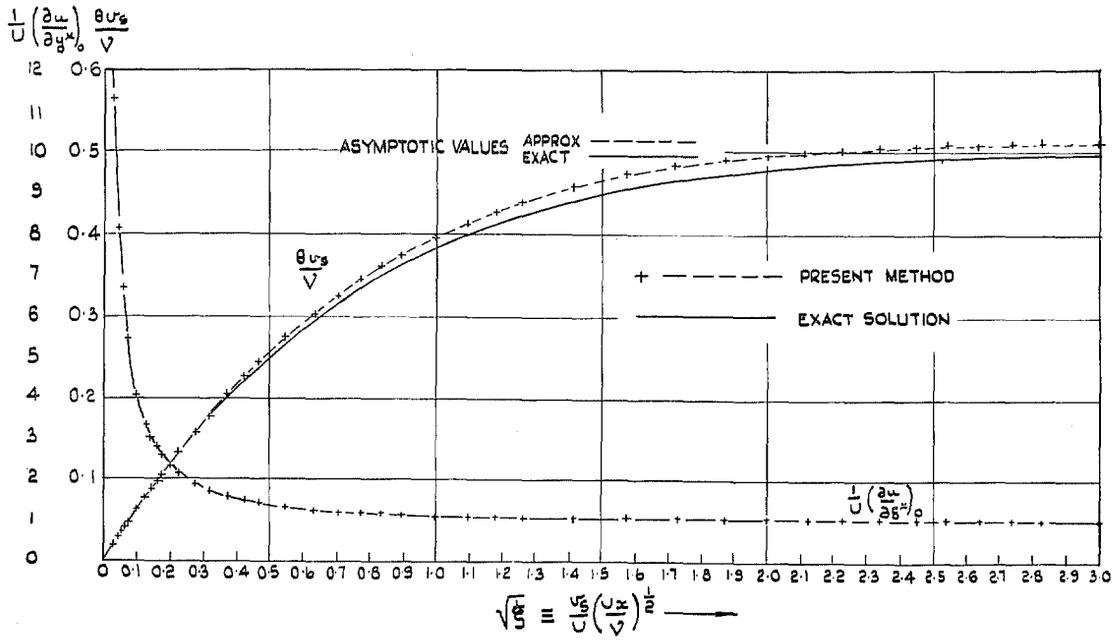

FIG. 30. Variation of skin friction and momentum thickness along flat plate with uniform suction.

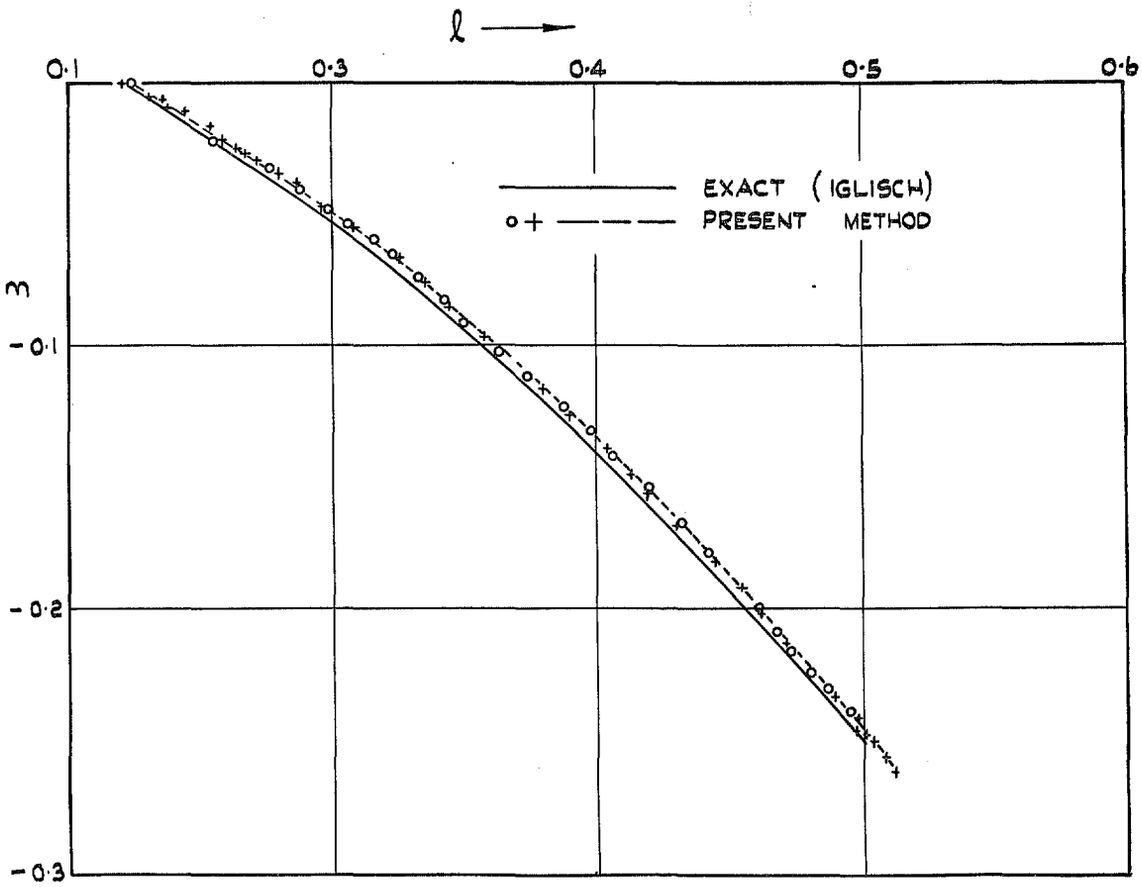

FIG. 31. l, m curves for exact and approximate calculations.

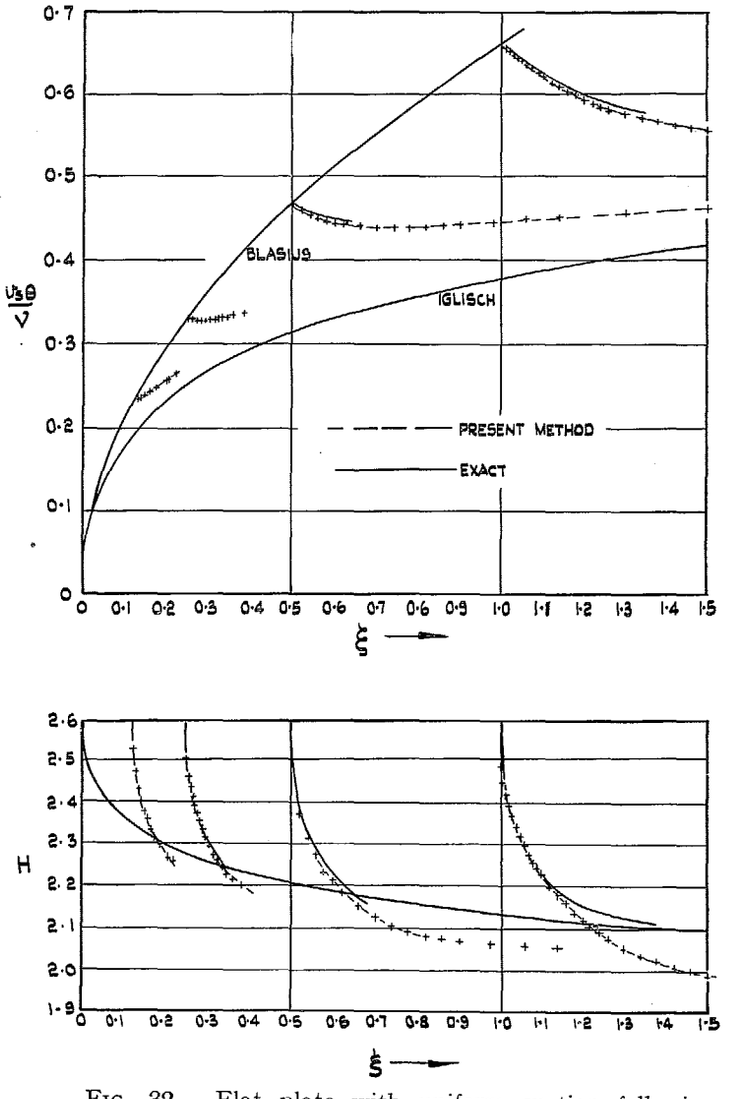

FIG. 32. Flat plate with uniform suction following solid-entry length.

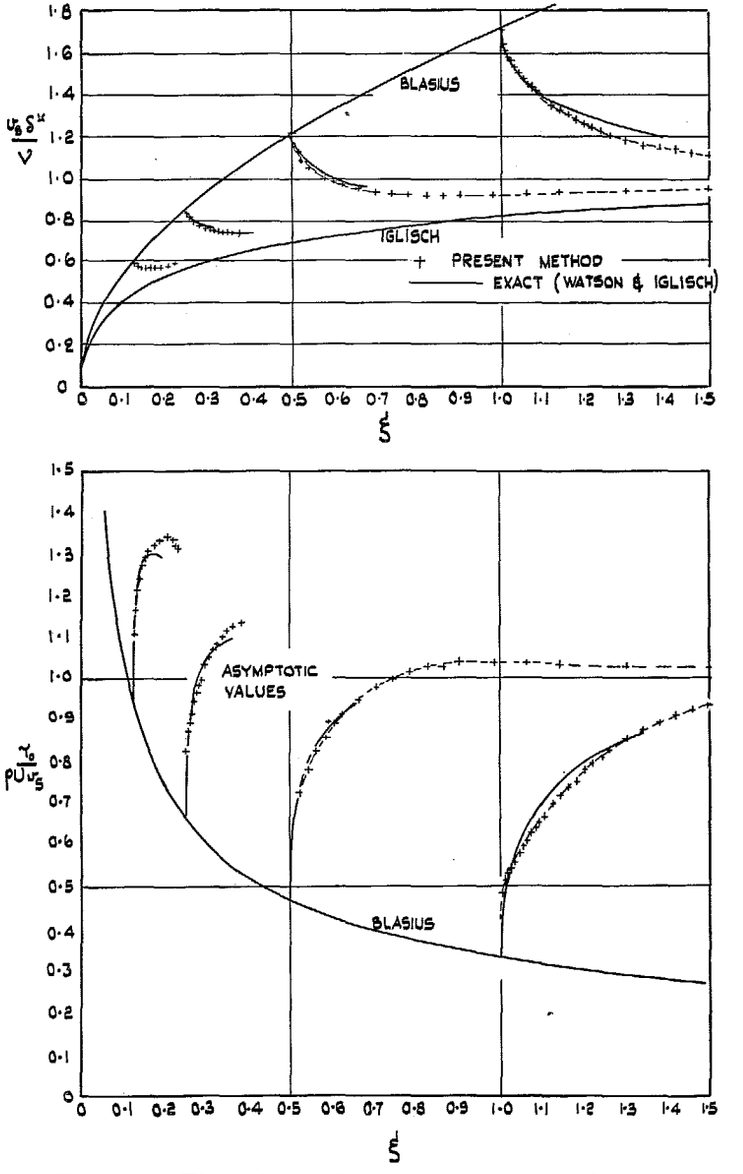

FIG. 33. Flat plate with uniform suction following solid-entry length.

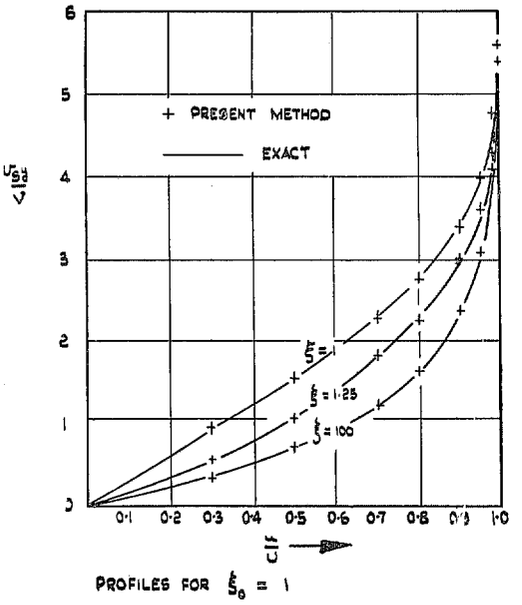

FIG. 34. Flat plate with uniform suction following solid-entry length.

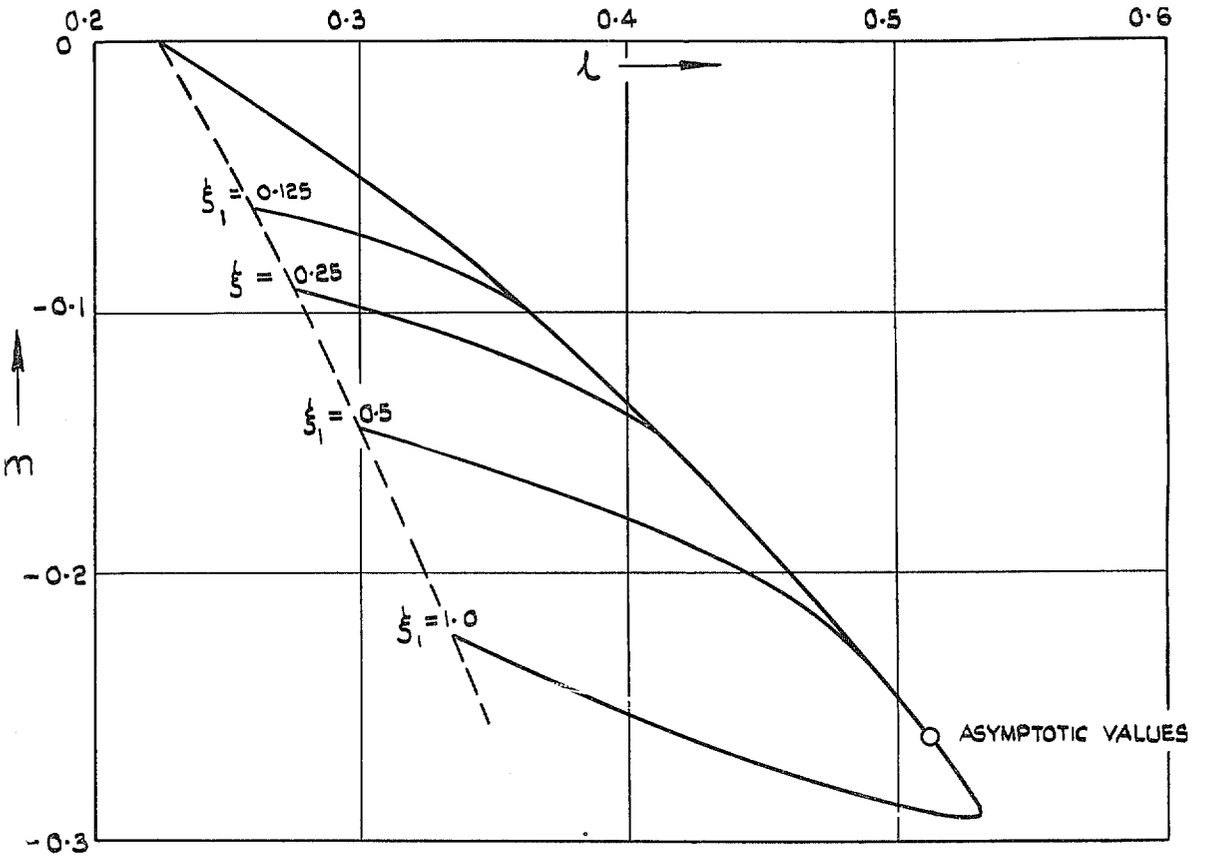

FIG. 35. Flat plate with uniform suction following solid-entry length.

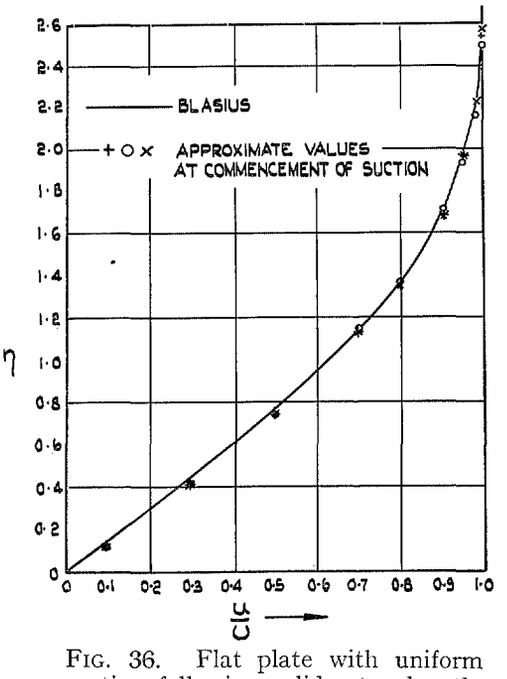

FIG. 36. Flat plate with uniform suction following solid-entry length.

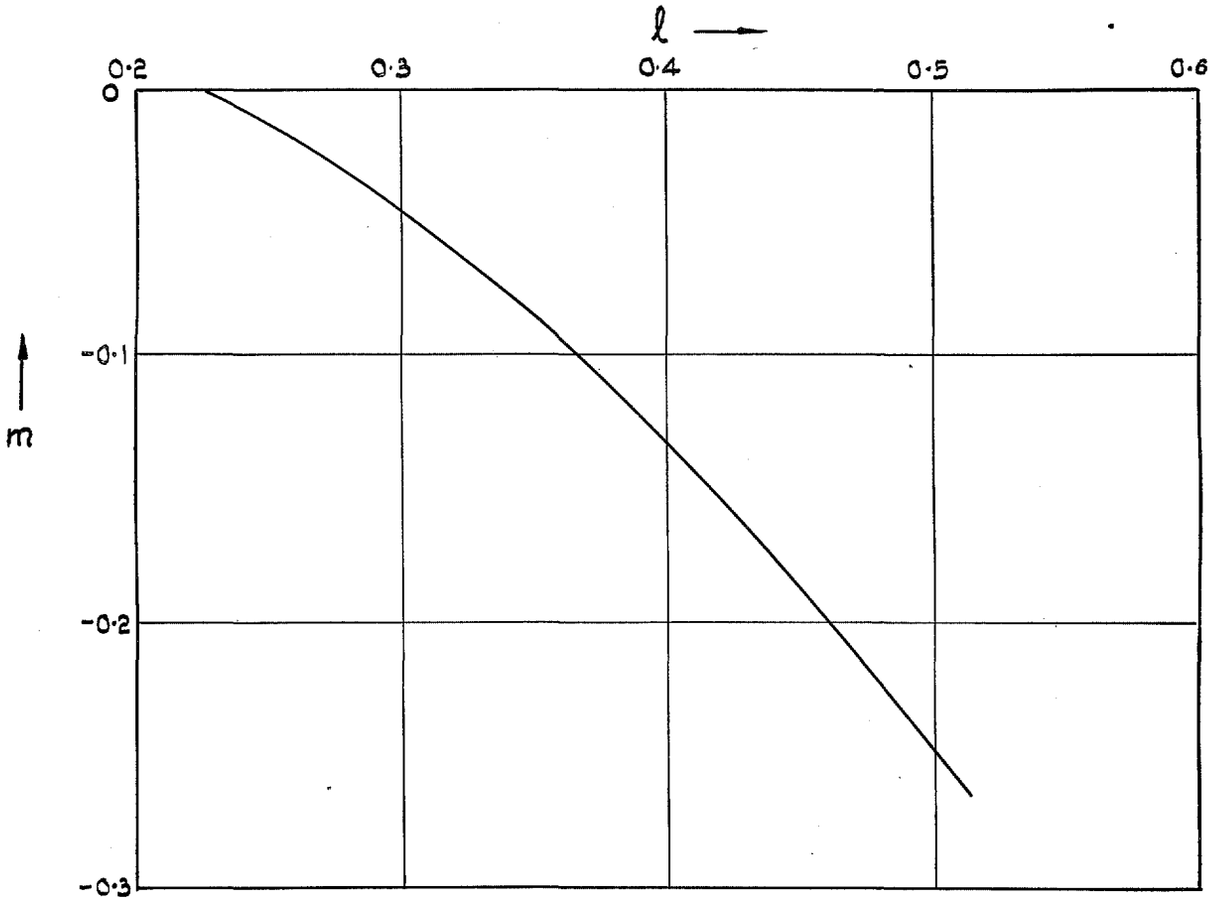

FIG. 37. Flat plate with $v_s \propto x^{-1/2}$.

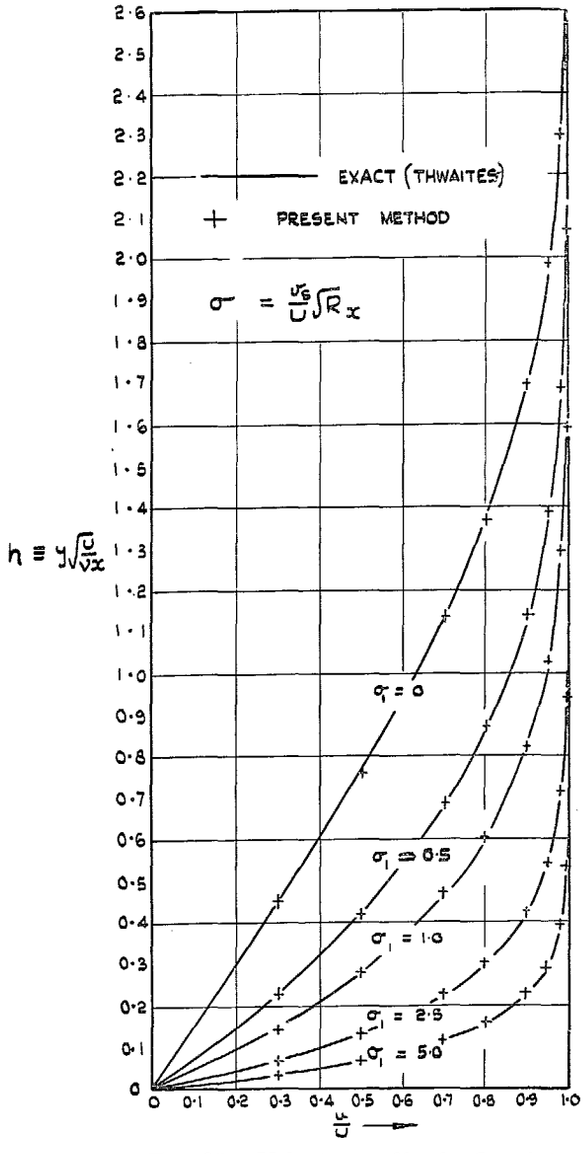

FIG. 38. Velocity profiles for flat plate with $v_s \propto x^{-1/2}$

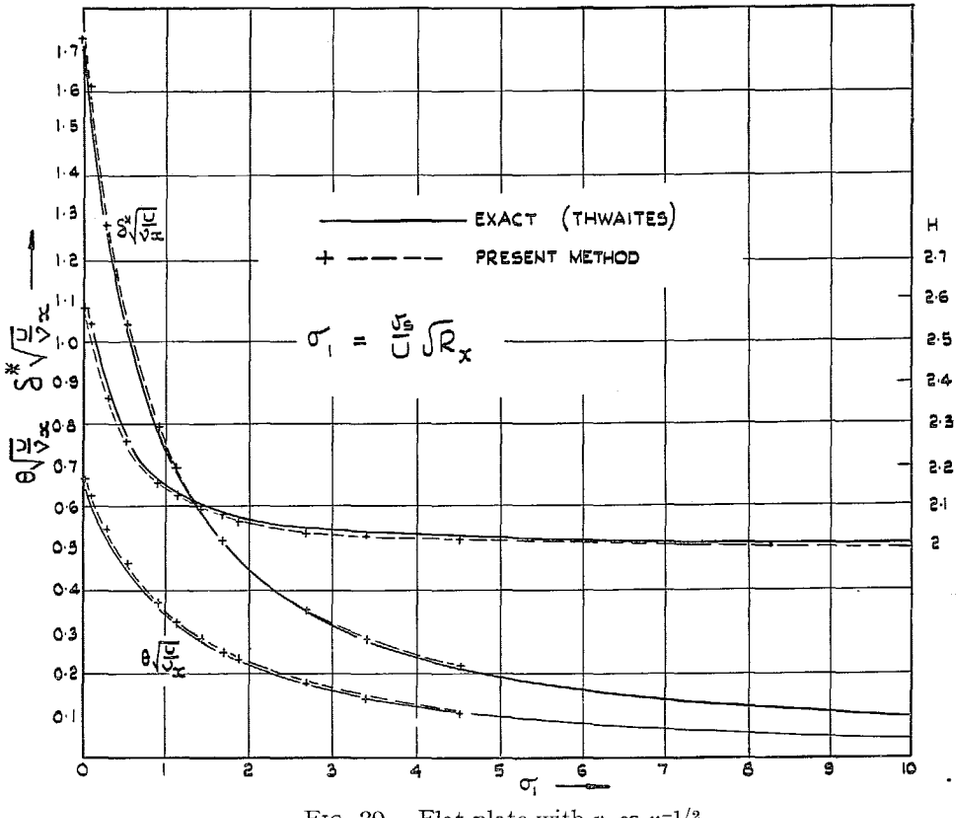

FIG. 39. Flat plate with $v_s \propto x^{-1/2}$.

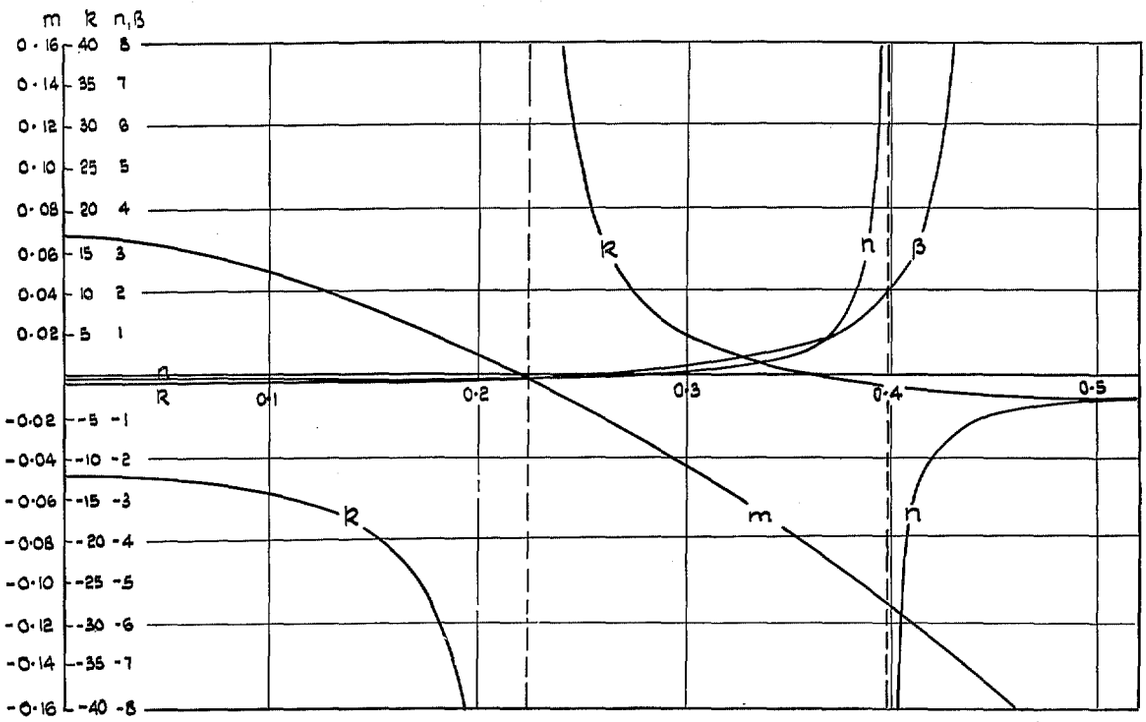

FIG. 40. m, k, n and β as functions of l for flow $U = Cx^n$.

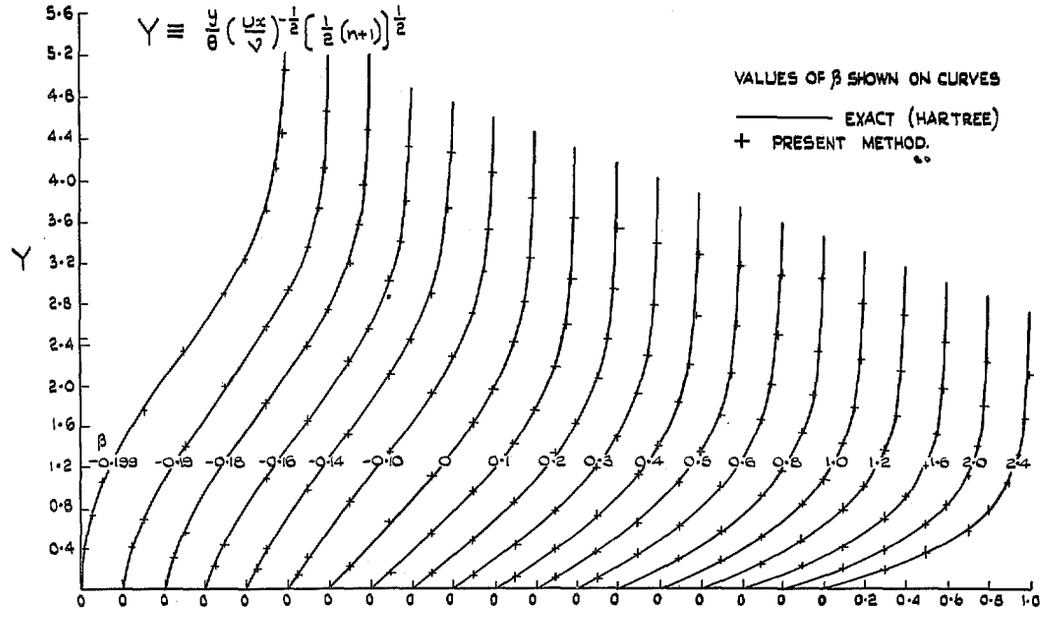

FIG. 41. Boundary-layer velocity profiles for flow $U = Cx^n$.

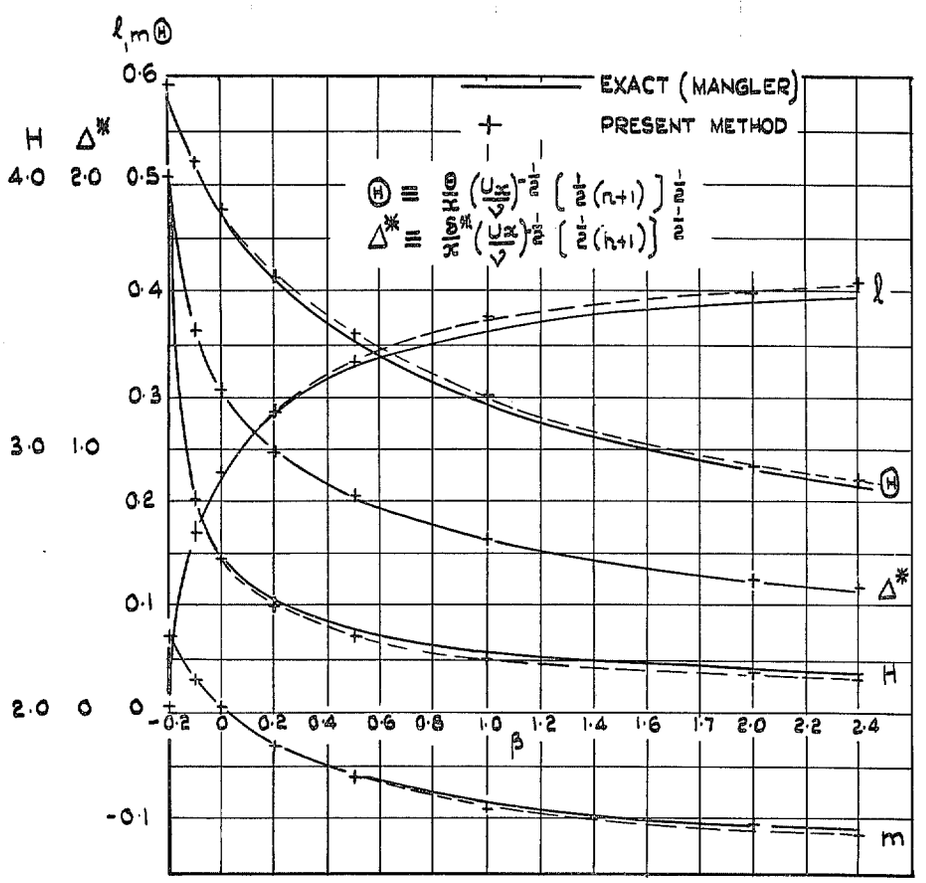

FIG. 42. Characteristics of profiles for flow $U = Cx^n$.

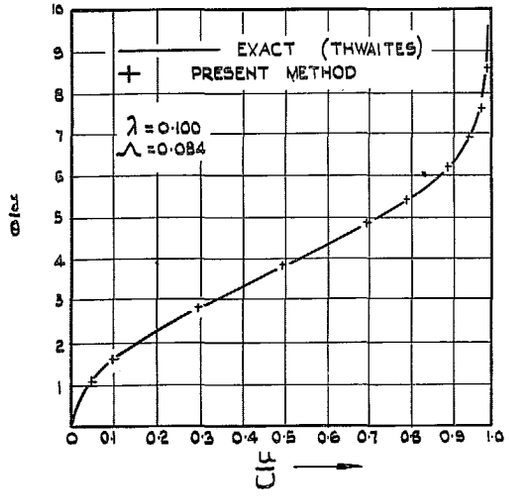

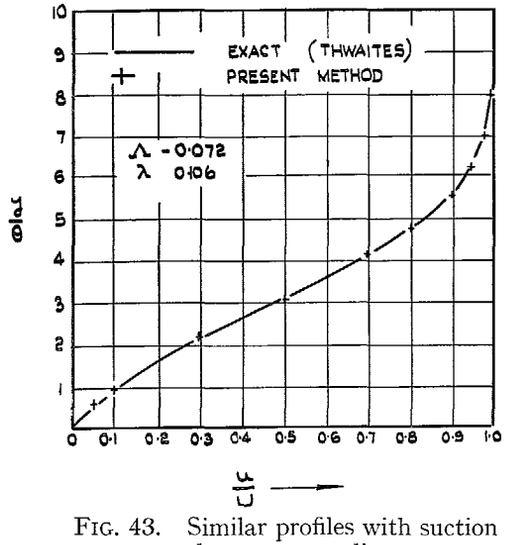

FIG. 43. Similar profiles with suction and pressure gradient.

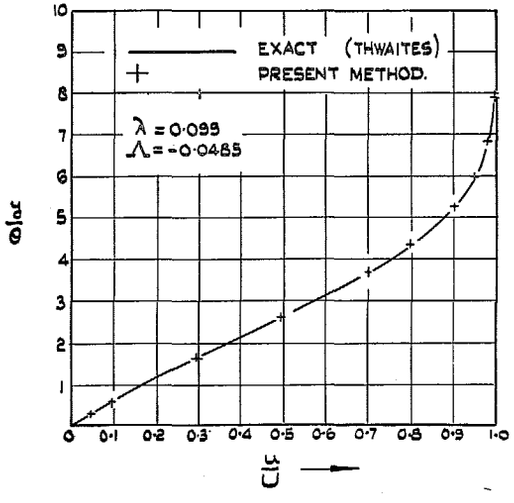

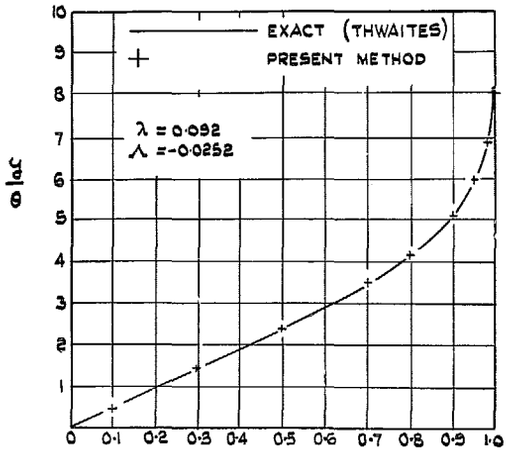

FIG. 44. Similar profiles with suction and pressure gradient.

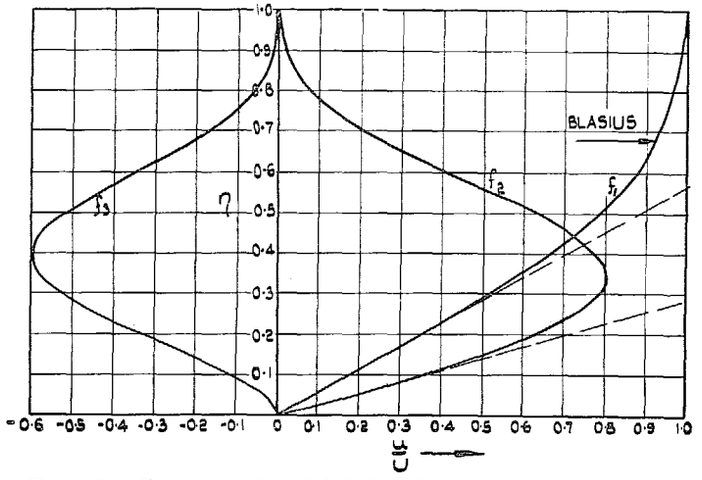

FIG. 45. Functions f_1 and f_2 & f_3 as determined at separation.

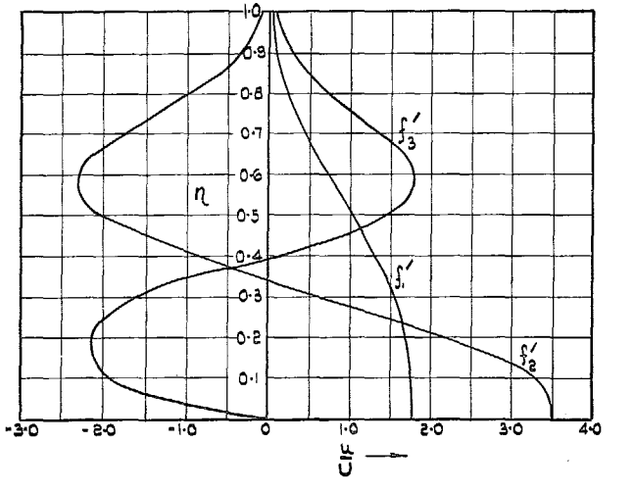

FIG. 47. f_1' and f_2' & f_3' as determined at separation.

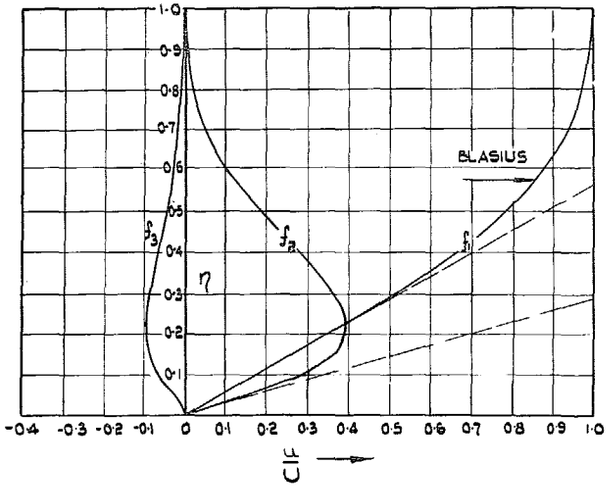

FIG. 46. Functions f_1 and f_2 & f_3 as determined from profiles with high skin friction.

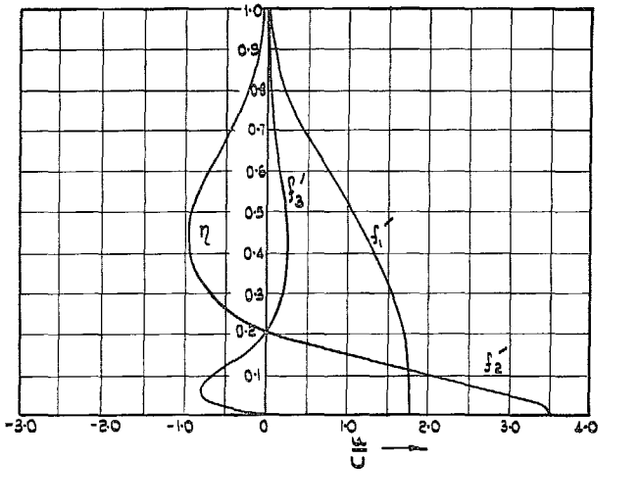

FIG. 48. f_1' and f_2' & f_3' as determined from profiles with high skin friction.

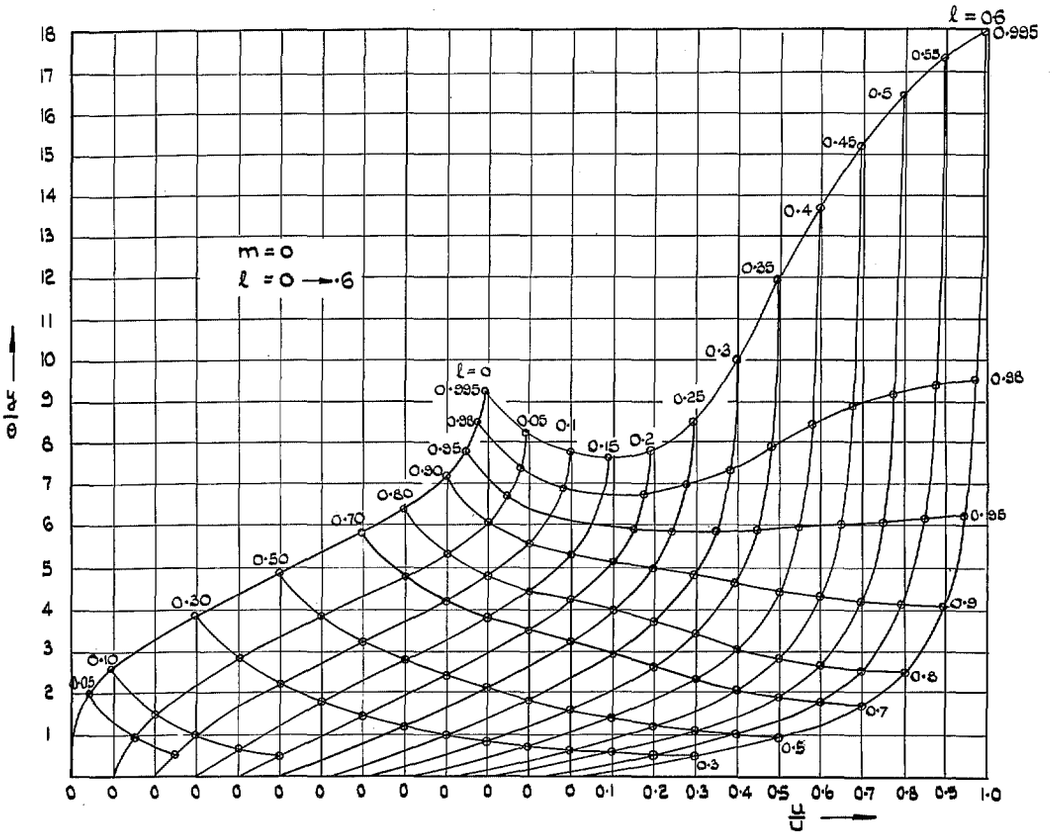

FIG. 49. Velocity profiles $m \leqslant 0$ (i).

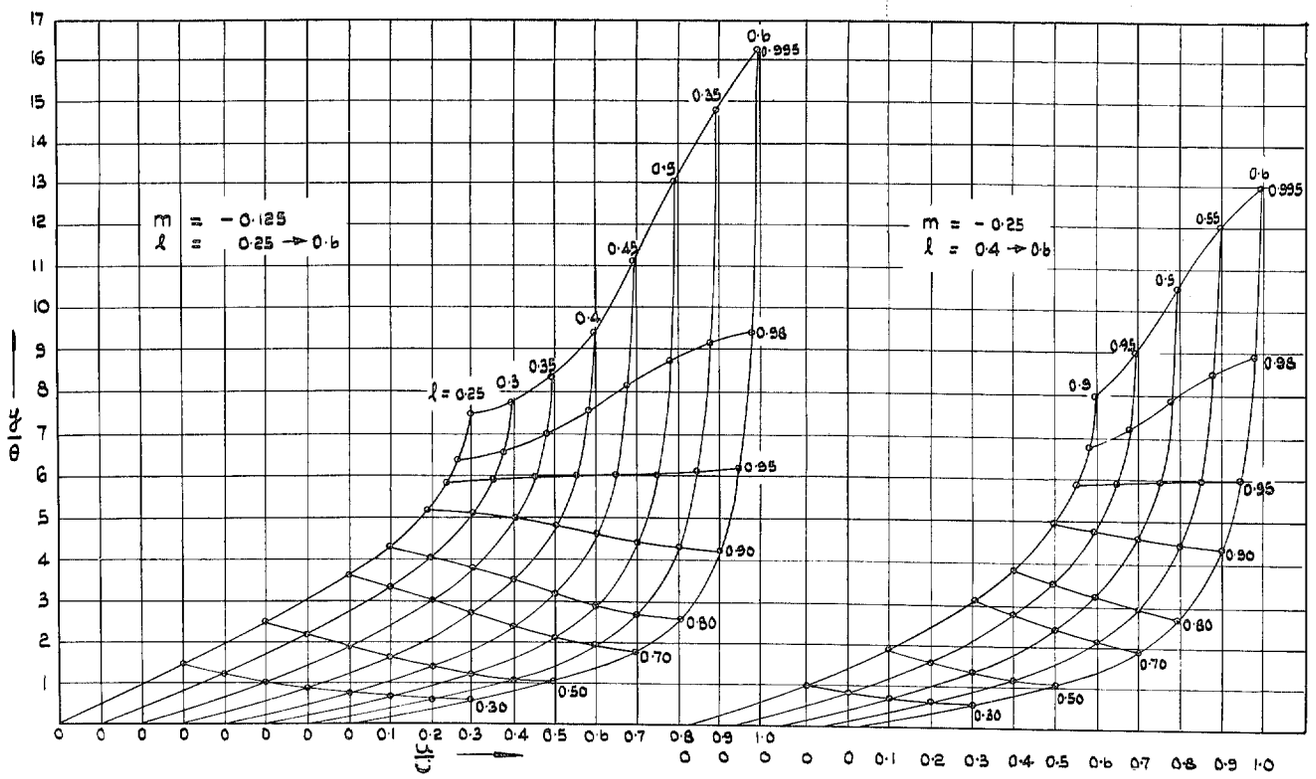

FIG. 50. Profiles $m \leqslant 0$ (ii).

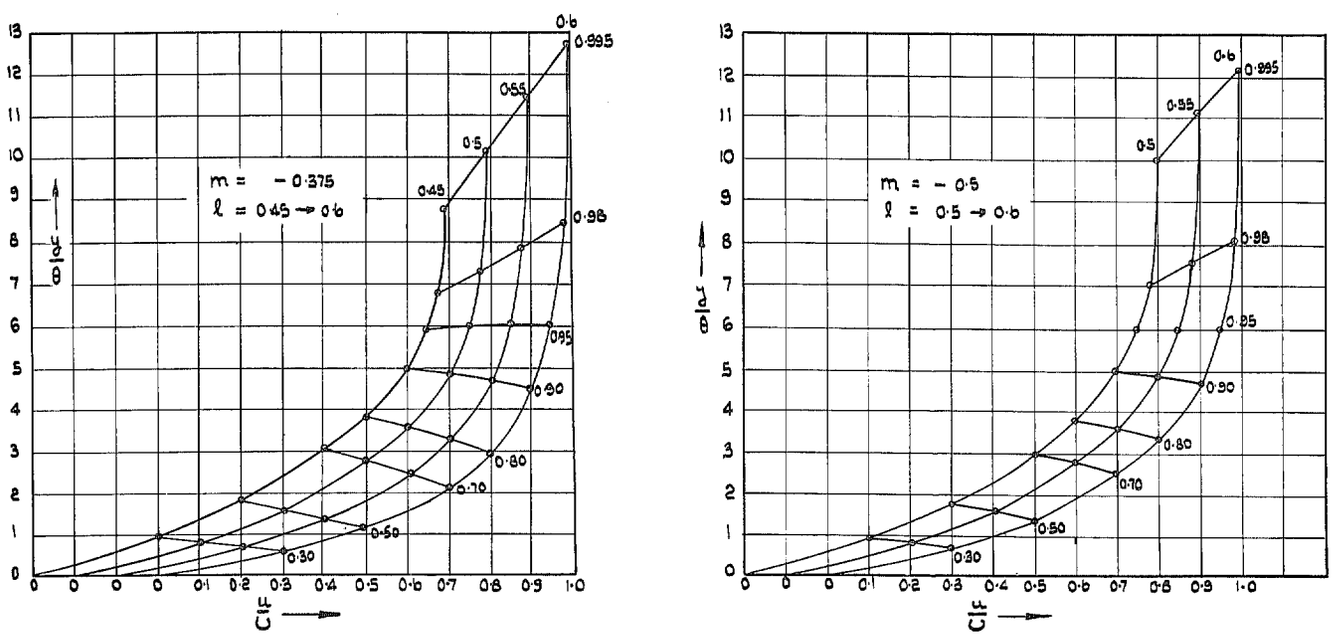

FIG. 51. Profiles $m \leqslant 0$ (iii).

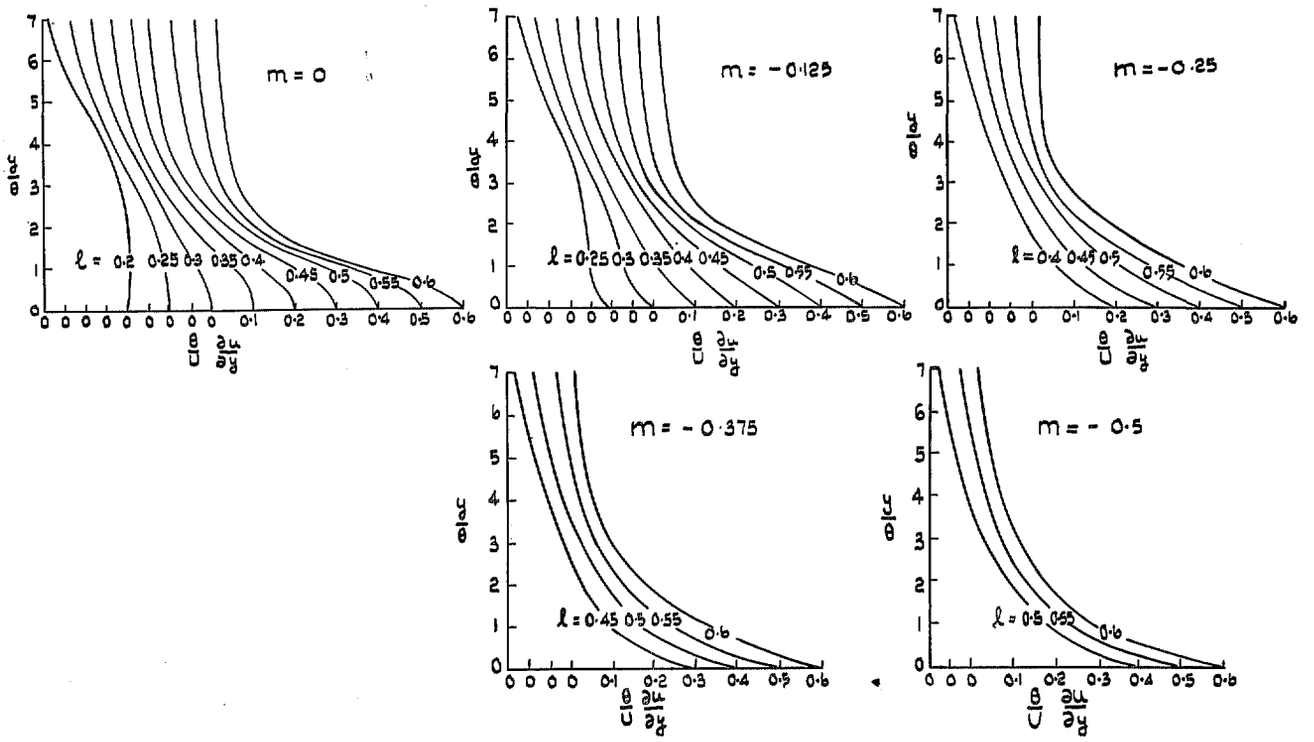

FIG. 52. Profiles of $(\theta/U)(\partial u/\partial y)$.

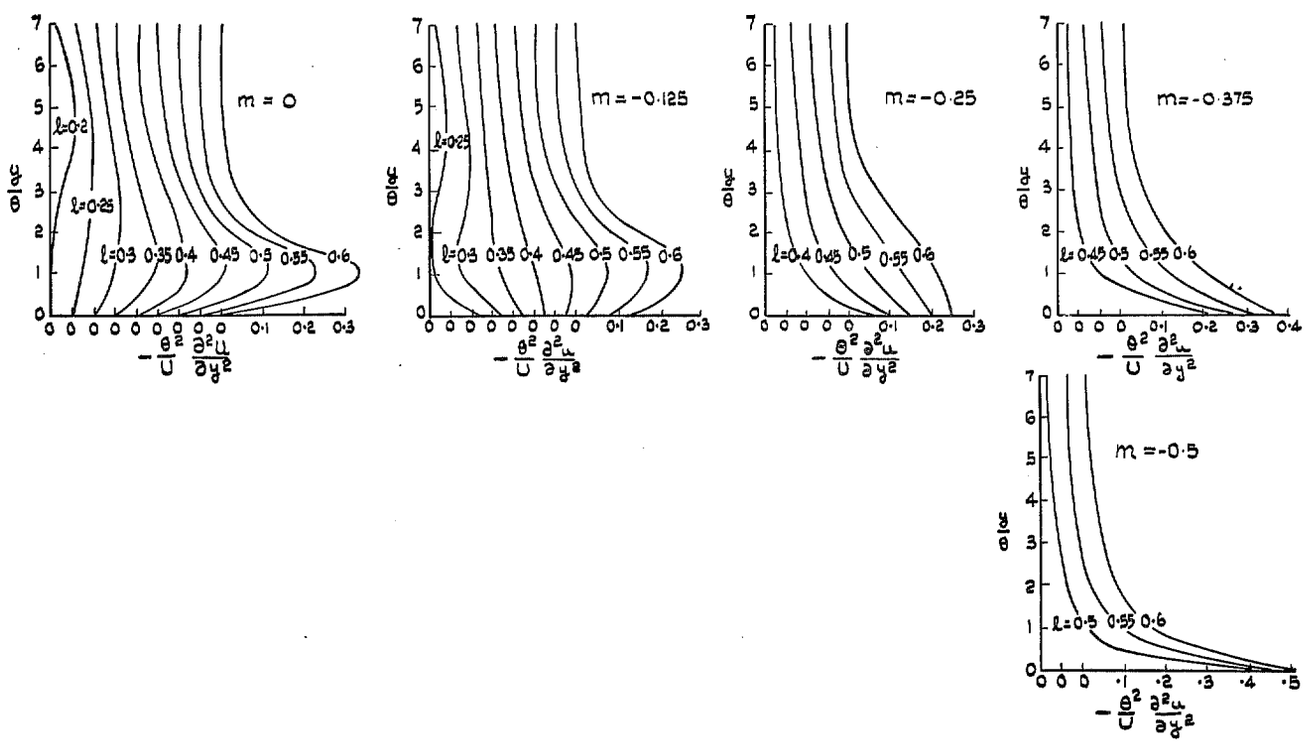

FIG. 53. Profiles of $(\theta^2/U)(\partial^2 u/\partial y^2)$.

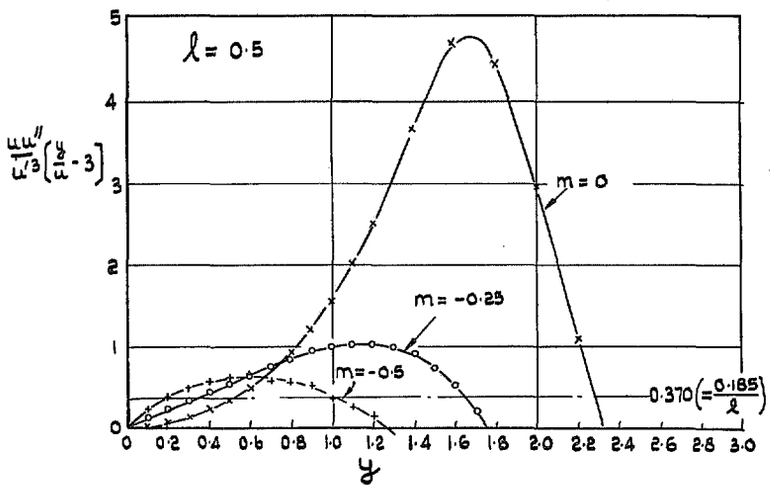

FIG. 54. Roots of equation (5) found graphically.

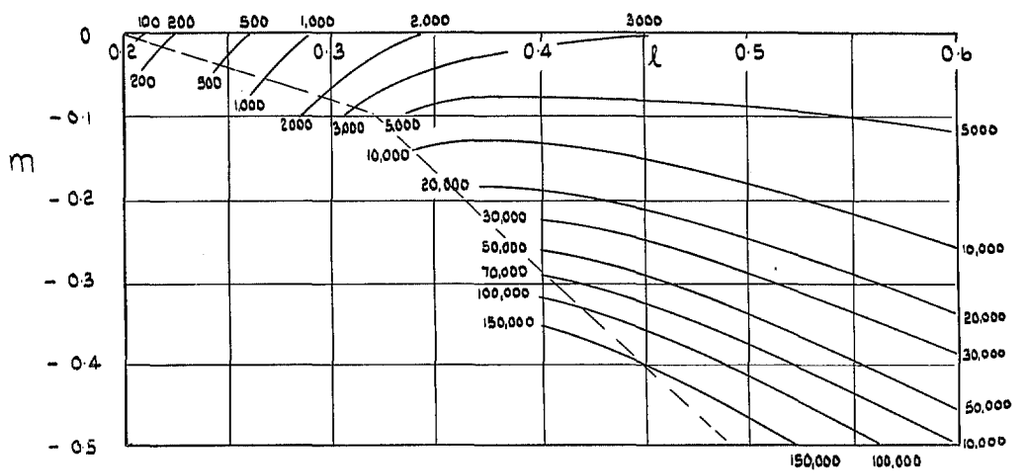

FIG. 55. $R_{0\,\mathrm{crit}}$ plotted as a function of l and m.

(75237) Wt. 53/2293 K7 9/59 Hw.

PRINTED IN GREAT BRITAIN

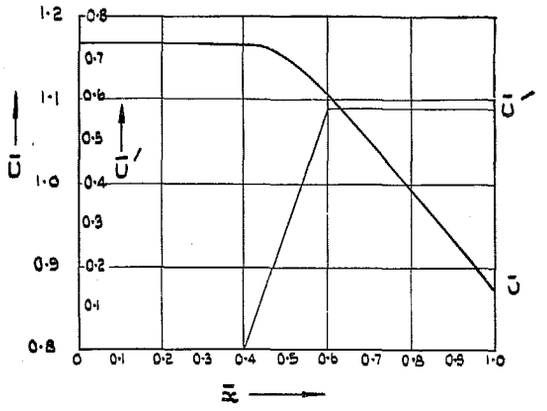

FIG. 56. Distributions of velocity and velocity gradient.

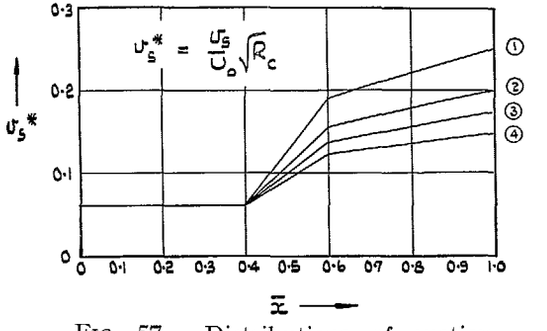

FIG. 57. Distributions of suction velocity.

FIGS. 56 and 57. Upper surface of 10 per cent thick aerofoil.

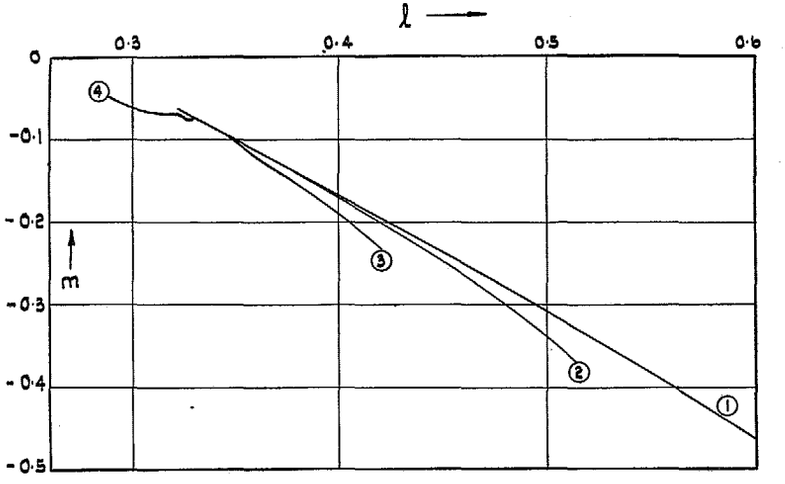

FIG. 58. l, m curves.

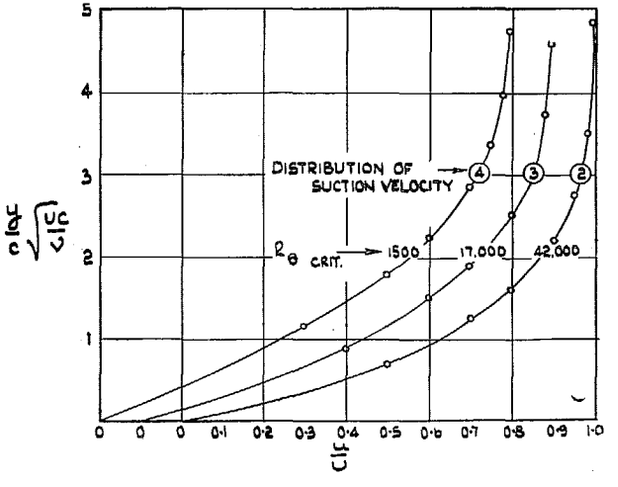

FIG. 59. Velocity profiles at trailing edge.

FIGS. 58 and 59. Calculations for upper surface of 10 per cent thick aerofoil.

Publications of the Aeronautical Research Council

ANNUAL TECHNICAL REPORTS OF THE AERONAUTICAL RESEARCH COUNCIL (BOUND VOLUMES)

1939 Vol. I. Aerodynamics General, Performance, Airscrews, Engines. 50*s*. (52*s*.).
Vol. II. Stability and Control, Flutter and Vibration, Instruments, Structures, Seaplanes, etc. 63*s*. (65*s*.)

1940 Aero and Hydrodynamics, Aerofoils, Airscrews, Engines, Flutter, Icing, Stability and Control, Structures, and a miscellaneous section. 50*s*. (52*s*.)

1941 Aero and Hydrodynamics, Aerofoils, Airscrews, Engines, Flutter, Stability and Control, Structures. 63*s*. (65*s*.)

1942 Vol. I. Aero and Hydrodynamics, Aerofoils, Airscrews, Engines. 75*s*. (77*s*.)
Vol. II. Noise, Parachutes, Stability and Control, Structures, Vibration, Wind Tunnels. 47*s*. 6*d*. (49*s*. 6*d*.)

1943 Vol. I. Aerodynamics, Aerofoils, Airscrews. 80*s*. (82*s*.)
Vol. II. Engines, Flutter, Materials, Parachutes, Performance, Stability and Control, Structures. 90*s*. (92*s*. 9*d*.)

1944 Vol. I. Aero and Hydrodynamics, Aerofoils, Aircraft, Airscrews, Controls. 84*s*. (86*s*. 6*d*.)
Vol. II. Flutter and Vibration, Materials, Miscellaneous, Navigation, Parachutes, Performance, Plates and Panels, Stability, Structures, Test Equipment, Wind Tunnels. 84*s*. (86*s*. 6*d*.)

1945 Vol. I. Aero and Hydrodynamics, Aerofoils. 130*s*. (132*s*. 9*d*.)
Vol. II. Aircraft, Airscrews, Controls. 130*s*. (132*s*. 9*d*.)
Vol. III. Flutter and Vibration, Instruments, Miscellaneous, Parachutes, Plates and Panels, Propulsion. 130*s*. (132*s*. 6*d*.)
Vol. IV. Stability, Structures, Wind Tunnels, Wind Tunnel Technique. 130*s*. (132*s*. 6*d*.)

Annual Reports of the Aeronautical Research Council—

1937 2*s*. (2*s*. 2*d*.) 1938 1*s*. 6*d*. (1*s*. 8*d*.) 1939–48 3*s*. (3*s*. 5*d*.)

Index to all Reports and Memoranda published in the Annual Technical Reports, and separately—

April, 1950 - - - - R. & M. 2600 2*s*. 6*d*. (2*s*. 10*d*.)

Author Index to all Reports and Memoranda of the Aeronautical Research Council—

1909—January, 1954 R. & M. No. 2570 15*s*. (15*s*. 8*d*.)

Indexes to the Technical Reports of the Aeronautical Research Council—

December 1, 1936—June 30, 1939	R. & M. No. 1850	1*s*. 3*d*. (1*s*. 5*d*.)
July 1, 1939—June 30, 1945	R. & M. No. 1950	1*s*. (1*s*. 2*d*.)
July 1, 1945—June 30, 1946	R. & M. No. 2050	1*s*. (1*s*. 2*d*.)
July 1, 1946—December 31, 1946	R. & M. No. 2150	1*s*. 3*d*. (1*s*. 5*d*.)
January 1, 1947—June 30, 1947	R. & M. No. 2250	1*s*. 3*d*. (1*s*. 5*d*.)

Published Reports and Memoranda of the Aeronautical Research Council—

Between Nos. 2251–2349	R. & M. No. 2350	1*s*. 9*d*. (1*s*. 11*d*.)
Between Nos. 2351–2449	R. & M. No. 2450	2*s*. (2*s*. 2*d*.)
Between Nos. 2451–2549	R. & M. No. 2550	2*s*. 6*d*. (2*s*. 10*d*.)
Between Nos. 2551–2649	R. & M. No. 2650	2*s*. 6*d*. (2*s*. 10*d*.)
Between Nos. 2651–2749	R. & M. No. 2750	2*s*. 6*d*. (2*s*. 10*d*.)

Prices in brackets include postage

HER MAJESTY'S STATIONERY OFFICE

York House, Kingsway, London W.C.2; 423 Oxford Street, London W.1; 13a Castle Street, Edinburgh 2; 39 King Street, Manchester 2; 2 Edmund Street, Birmingham 3; 109 St. Mary Street, Cardiff; Tower Lane, Bristol 1; 80 Chichester Street, Belfast, *or through any bookseller.*

S.O. Code No. 23-3123